# NAVAL POSTGRADUATE SCHOOL
## Monterey, California

UNITED STATES NAVY · NAVAL POSTGRADUATE SCHOOL

DTIC
S ELECTE
MAR 12 1991
B D

# THESIS

EVALUATION OF GENERALIZED THRESHOLDS
IN AN OBJECTIVE MULTISPECTRAL
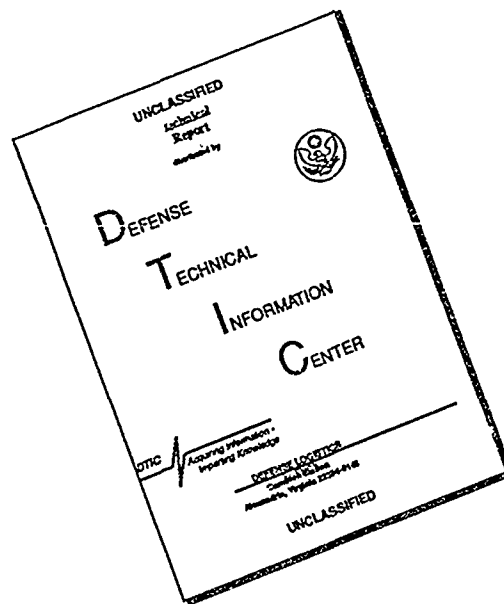SATELLITE CLOUD ANALYSIS

by

Thomas J. Neu

June 1990

Thesis Advisor          Carlyle H. Wash

91 3 06 030

# DISCLAIMER NOTICE

UNCLASSIFIED
Technical
Report
distributed by

**D**EFENSE

**T**ECHNICAL

**I**NFORMATION

**C**ENTER

DTIC / Acquiring Information ·
Imparting Knowledge

DEFENSE LOGISTICS
Cameron Station
Alexandria, Virginia 22304-6145

UNCLASSIFIED

THIS DOCUMENT IS BEST
QUALITY AVAILABLE. THE COPY
FURNISHED TO DTIC CONTAINED
A SIGNIFICANT NUMBER OF
PAGES WHICH DO NOT
REPRODUCE LEGIBLY.

## REPORT DOCUMENTATION PAGE

| | | | |
|---|---|---|---|
| 1a Report Security Classification Unclassified | | 1b Restrictive Markings | |
| 2a Security Classification Authority | | 3 Distribution Availability of Report | |
| 2b Declassification Downgrading Schedule | | Approved for public release; distribution is unlimited. | |
| 4 Performing Organization Report Number(s) | | 5 Monitoring Organization Report Number(s) | |
| 6a Name of Performing Organization Naval Postgraduate School | 6b Office Symbol (if applicable) 35 | 7a Name of Monitoring Organization Naval Postgraduate School | |
| 6c Address (city, state, and ZIP code) Monterey, CA 93943-5000 | | 7b Address (city, state, and ZIP code) Monterey, CA 93943-5000 | |
| 8a Name of Funding Sponsoring Organization | 8b Office Symbol (if applicable) | 9 Procurement Instrument Identification Number | |
| 8c Address (city, state, and ZIP code) | | 10 Source of Funding Numbers | |
| | | Program Element No / Project No / Task No / Work Unit Accession No | |

11 Title (include security classification) EVALUATION OF GENERALIZED THRESHOLDS IN AN OBJECTIVE MULTI-SPECTRAL SATELLITE CLOUD ANALYSIS

12 Personal Author(s) Thomas J. Neu

| 13a Type of Report Master's Thesis | 13b Time Covered From      To | 14 Date of Report (year, month, day) June 1990 | 15 Page Count 60 |
|---|---|---|---|

16 Supplementary Notation The views expressed in this thesis are those of the author and do not reflect the official policy or position of the Department of Defense or the U.S. Government.

| 17 Cosati Codes | | | 18 Subject Terms (continue on reverse if necessary and identify by block number) |
|---|---|---|---|
| Field | Group | Subgroup | Meteorology, Satellite Remote Sensing, Automated Nephanalysis, Multispectral Thresholding |
| | | | |
| | | | |

19 Abstract (continue on reverse if necessary and identify by block number) An objective algorithm is developed and evaluated for classifying 11 cloud types using a minicomputer. The multispectral technique uses daytime images of AVHRR channel 1 (0.68 $\mu m$), channel 4 (10.8 $\mu m$) and channel 5 (12.0 $\mu m$). Visual reflectance is scaled by the solar zenith angle in order to prepare standardized albedos. Infrared brightness temperatures provide cloud height information through comparison with a representative temperature sounding. Channel 4-5 temperature differences (split-window) distinguish between ice clouds with variable emissivities and thick precipitating clouds. A statistical texture analysis on the standardized albedos separates stratiform from cumuliform clouds. Generalized thresholds were set for each of these parameters to discriminate between cloud types. The evaluation judges model performance based on four case studies located at different latitudes with varying solar zenith angles. Overall results compiled between the cases show a 67% agreement for manual and model classifications General results compiled for clear, low clouds, middle clouds, high clouds and precipitation cloud types were even more successful with 94%, 90%, 50%, 87% and 95% agreement, respectively. The color enhanced automated product provides a legible, quick and accurate tool for cloud type analysis.

| 20 Distribution Availability of Abstract ☒ unclassified unlimited ☐ same as report ☐ DTIC users | 21 Abstract Security Classification Unclassified | |
|---|---|---|
| 22a Name of Responsible Individual Carlyle H. Wash | 22b Telephone (include Area code) (408) 646-2295 | 22c Office Symbol MR/WX |

Evaluation of Generalized Thresholds
in an Objective Multispectral
Satellite Cloud Analysis

by

Thomas J. Neu
Captain, United States Air Force
B.S., University of New Hampshire, 1981
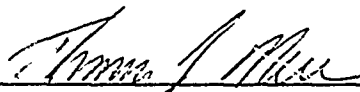B.S., North Carolina State University, 1985

Submitted in partial fulfillment of the
requirements for the degree of

MASTER OF SCIENCE IN METEOROLOGY

from the

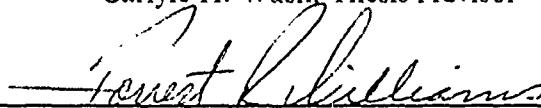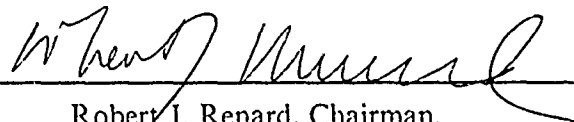NAVAL POSTGRADUATE SCHOOL
June 1990

Author: _____
Thomas J. Neu

Approved by: _____
Carlyle H. Wash, Thesis Advisor

_____
Forrest R. Williams, Second Reader

_____
Robert J. Renard, Chairman,
Department of Meteorology

ii

# ABSTRACT

An objective algorithm is developed and evaluated for classifying 11 cloud types using a minicomputer. The multispectral technique uses daytime images of AVHRR channel 1 (0.68 $\mu$m), channel 4 (10.8 $\mu$m) and channel 5 (12.0 $\mu$m). Visual reflectance is scaled by the solar zenith angle in order to prepare standardized albedos. Infrared brightness temperatures provide cloud height information through comparison with a representative temperature sounding. Channel 4-5 temperature differences (split-window) distinguish between ice clouds with variable emissivities and thick precipitating clouds. A statistical texture analysis on the standardized albedos separates stratiform from cumuliform clouds. Generalized thresholds were set for each of these parameters to discriminate between cloud types. The evaluation judges model performance based on four case studies located at different latitudes with varying solar zenith angles. Overall results compiled between the cases show a 67% agreement for manual and model classifications. General results compiled for clear, low clouds, middle clouds, high clouds and precipitation cloud types were even more successful with 94%, 90%, 50%, 87% and 95% agreement, respectively. The color enhanced automated product provides a legible, quick and accurate tool for cloud type analysis.

# TABLE OF CONTENTS

# LIST OF TABLES

# LIST OF FIGURES

## ACKNOWLEDGEMENTS

# I. INTRODUCTION

Interest in objectively determining cloud types from satellite data began in 1960 with the launch of the TIROS series satellites. Early nephanalysis products were produced manually, in a time intensive and subjective manner. The meteorologist classified clouds based on pattern recognition and brightness intensities discerned from a visual and infrared image. Today's remote imaging systems have enhanced our ability to distinguish between cloud types by incorporating additional visual and infrared spectral channels and increasing their spatial resolution. The advent of computer technology over the last decade provides meteorologists with an efficient and needed tool for handling the millions of binary elements contained in a single satellite scene. The ability to process and display the digital data stream from satellites rapidly and in a convenient form lends itself to an automated nephanalysis.

The need for better cloud type information is found in a variety of disciplines. Meteorological forecasting, military operations, energy and moisture budget analysis and modeling, climatological research and hydrological studies all require an accurate spatial and temporal knowledge of cloud amount and types. The performance of optical guidance systems used for navigation and targeting information on sophisticated weaponry is highly dependent on cloud parameters. Strategic and tactical reconnaissance also requires accurate and detailed cloud information for planning purposes and operational decision making. Different types of clouds have different radiational properties and moisture characteristics, which play a crucial role in the accurate parameterization of advanced numerical models being developed to more accurately predict atmospheric phenomena. Studies concerning global climatic change require an understanding and comprehensive portrayal of the earth's cloud distribution in order to formulate meaningful conclusions regarding future conditions. The range and multiplicity of potential users indicate that a formal, standardized nephanalysis program is needed. The growing volume of available satellite, conventional and numerical model data dictates that a successful method will be automated and interactive.

The objective of this thesis is to evaluate an automated multispectral nephanalysis model utilizing the Interactive Digital Environmental Analysis (IDEA) Laboratory minicomputer at the Naval Postgraduate School. The model used is a revision of Nelson's (1982) automated cloud model, which employs Liljas' (1982) cloud threshold

1

intensity box scheme and the Harris and Barrett (1978) statistical cloud texture technique. Visual and infrared digital satellite data from the Advanced Very High Resolution Radiometer (AVHRR) sensor flown on the National Oceanic and Atmospheric Administration (NOAA) polar orbiting satellites is used for the analysis. The evaluation focuses on the effect that latitudinal and solar zenith angle variations have on the accuracy of the objective analysis. The results will determine the feasibility of using the model to produce an operational regional nephanalysis product that can be used in a global context. The verification procedure will show the strengths and weaknesses in the classification procedures for the 11 different cloud types analyzed by the model.

Chapter II will present information on recent approaches and research involving automated cloud analysis from digital satellite data. This will set the framework for the evaluated model's derivation, and provide insight to the benefits and limitations of an automated cloud analysis. Chapter III describes the multispectral model used for the nephanalysis. The satellite system, model algorithm and characteristics of the cloud types to be differentiated will be discussed. A brief review of the radiative transfer principals and the means of obtaining threshold values used in the model will also be presented. Chapter IV will present the data description for the case studies and outline the approach employed for the evaluation. Results and findings of the evaluation will follow in Chapter V. Conclusions and recommendations for further investigation will be discussed in Chapter VI.

## II. BACKGROUND

The usual method for identifying cloud types from satellite imagery is through manual interpretation. This is relatively easy for distinct cloud types, but the interpretation becomes complicated in systems composed of varying layers of different cloud types. The collocation of information and change in grey shade intensity between different satellite images introduce subjectivity to the manual interpretation. Automated cloud classification techniques use a computer to store, process and display the raw satellite imagery, and nephanalysis product. The subjectivity is taken out of the process by the computers ability to accurately collocate positions on different images and perform necessary calibration and standardization of grey shade intensity.

### A. BISPECTRAL CLOUD ANALYSIS

Reynolds and Vonder Haar (1976) developed a bispectral technique that quantitatively analyzes the visible and infrared data received at a contiguous array of scan spots using the NOAA Scanning Radiometer (SR). The product derived from this method includes both cloud amount and cloud top temperature. The cloud height then can be determined through a comparison with an appropriate nearby vertical temperature sounding. The bispectral technique also addresses the problem of determining cloud amount and height for cloud elements that are smaller than the spatial ground resolution of the sensor. Results obtained from ground truth surface observations at the White Sands Missile Range (WSMR) show good comparison for all cases except cirrus clouds. The suggested cause is the highly variable emissivity (0.10 - 0.95) of ice phase clouds.

The basis of the automated classification technique presented by Liljas (1982) is that cloud types and terrestrial surfaces have different radiational characteristics in different parts of the electromagnetic spectrum. Liljas suggests that the spectral channels on the AVHRR sensor could reveal the variation of radiative properties dictated by the cloud's height, phase of the cloud particles and density. Preliminary studies verified that brightness returns to the satellite correlated well with the radiational properties of different cloud and terrestrial types. A box classification scheme was developed, which identifies ten cloud types based on their visible and infrared return signatures. Fig. 1 depicts the main classifier in the model, where separation of different cloud types and terrestrial surfaces in a two dimensional intensity space are defined by the albedo derived

3
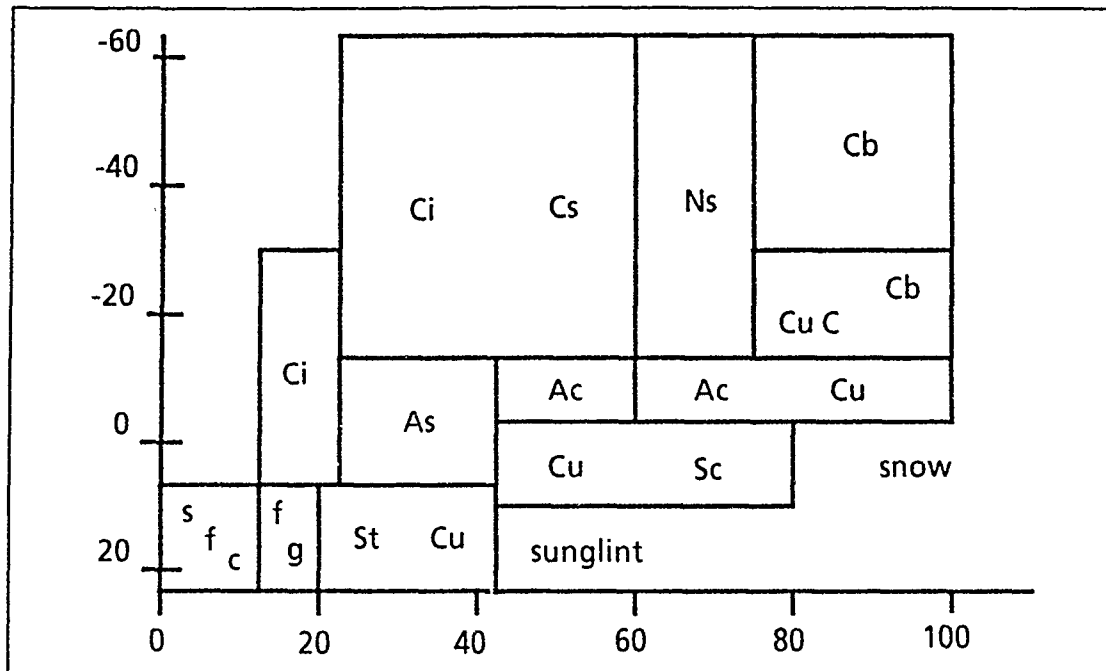
Fig. 1. Bispectral cloud classifier. From Liljas (1982), with albedo along the horizontal axis in % and temperature along the vertical axis in °C.

from visible channel 1 (0.63 $\mu$m) and temperature given by infrared channel 4 (11.0 $\mu$m).

Liljas' (1984) research was conducted during the summers of 1980 and 1981 over Sweden. Data collected from channels 1 through 4 by the AVHRR sensor on NOAA-6 and NOAA-7 polar orbiting satellites were used for his analysis. Liljas found that cloud classified images, using his automated box scheme, enabled forecasters to more effectively identify different classes of mesoscale cloud systems. He also concluded that a color enhanced nephanalysis display gave the forecaster a better understanding of the cloud structure in the various systems analyzed. The product greatly reduced the volume of satellite data requiring the forecasters attention, allowing him more time to formulate weather forecasts. Problems with his scheme include misclassification of cirrus cloud types, its restriction to daylight analysis, sun elevation distortion of albedo values and distinguishing between low clouds and snow/ice fields.

The Naval Postgraduate School (NPS) automated cloud and precipitation model produces an analysis of eight cloud types along with other important cloud and precipitation parameters. The model's performance has been evaluated by Moren (1984), Wyse (1984) and Spray (1985) using Geostationary Operational Environmental Satellite

4

(GOES) imagery from the Visual-Infrared Spin Scan Radiometer (VISSR). A detailed description of the model can be found in Wash et al. (1985). The bispectral classification uses infrared temperatures, visual albedos and visible standard deviation values to discriminate cloud types. The series of threshold tests follows Liljas's box scheme; it is shown in Fig. 2. Data input, basic satellite and statistical calculations, and cloud classification compose the three main processes in the model.

Five cases of GOES-East data over the eastern United States and western North Atlantic Ocean were used in evaluating the NPS model's performance. A fixed area of approximately 3000 X 3000 km was used in each case, with verification of the satellite derived cloud analysis based on conventional synoptic data, radar measurements and manual nephanalysis. The cloud type analyses were found to represent the general cloud patterns well, with statistical results of the evaluation listed in Wash et al. (1985). Most classification errors occurred in the direct comparison between satellite data and single station observations. Nimbostratus classification errors were primarily due to nimbostratus/altostratus boundaries located near the verification station, with surface observations of nimbostratus being misclassified as altostratus by the model. A majority of stratocumulus misclassifications were traced to errors in the textural decision, with the
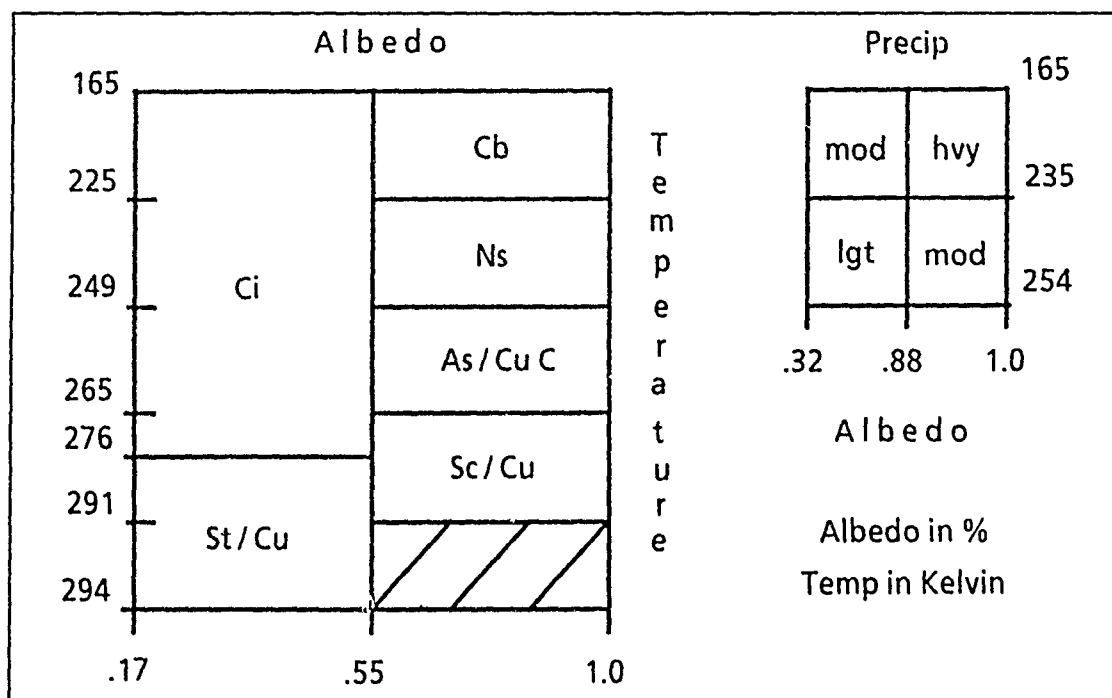
Fig. 2. NPS automated cloud model algorithm. From Wash et al. (1985), albedo in % and temperature in K.

model classifying stratocumulus as cumulus. Other classification errors occurred with small cumulus clouds that were smaller than the satellite field of view, thin cirrus clouds allowing surface radiation to be transmitted to the sensor and cumulus congestus, cumulonimbus which had warmer cloud tops than their respective set thresholds.

## B. TEXTURAL CLASSIFICATION

An automated classification technique was developed by Harris and Barrett (1978) using a statistical texture measurement for distinguishing stratiform from cumuliform clouds. They determined that both cloud brightness and cloud texture were the dominant factors when classifying cloud types in manual analysis, and thus should also dominate in automated nephanalysis schemes. A combination of brightness and texture analysis has proven successful in other remote sensing fields, such as identifying crop types (Maurer 1974) and terrain surfaces (Weszka et al. 1976). The method uses a computer to examine and quantify brightness and texture of small sub-arrays within the whole digital array picture. Through discriminate analysis, clouds are then identified as being either stratiform, cumuliform or of mixed types by a combination of brightness and texture values. Brightness values are derived using a standard mean calculation for the sub-array based on a density threshold defining the boundary between cloud and no-cloud values. A combination of standard deviation and vector dispersion calculations were used for determining the texture of the sub-array. These aggregates are then combined, producing an output map of cloud types. The sample texture values, and the boundaries produced from their training set by the application of the discriminant algorithm, is shown in Fig. 3.

The research performed by Harris and Barrett (1978) was conducted over western Europe during the spring of 1975 using high resolution Defense Meteorological Satellite Program (DMSP) imagery. They produced two separate nephanalysis, one using visual imagery and the other infrared, to type stratiform and cumuliform clouds. An assessment of the accuracy was formed by judging the automated products agreement with a corresponding expert manual nephanalysis. They concluded that the accuracy of the automatic classification was over 72 %. Problems found include classifying areas with towering cumuliform clouds as being clear, and with snow areas being misclassified as clouds. They believe that by increasing the resolution of the sub-array analysis cell from 40 km to 4 km, and using a multispectral approach, the accuracy of their classification would increase.

6
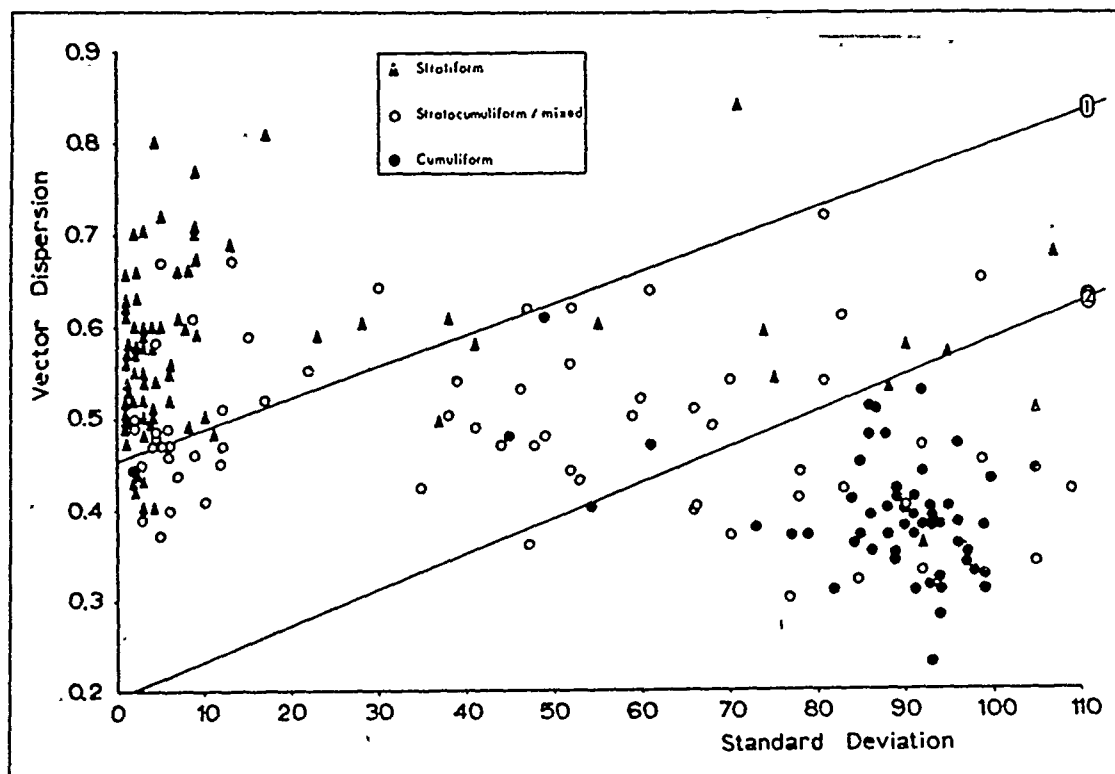
Fig. 3.    Linear discriminant analysis for cloud texture.    From Harris and Barrett (1978).

## C.  SPLIT WINDOW TECHNIQUE

A recurring problem in automated nephanalysis models is the misclassification of cirrus clouds, caused by the variability in emissivity of ice phased clouds.  Inoue (1987) addressed this problem and developed a split window technique for cirrus detection using infrared channels 4 (10.8 $\mu$m) and 5 (12.0 $\mu$m) of the AVHRR sensor.  The method is based on a threshold classification using brightness temperature differences (BTD) between split window channels.  The BTD is defined as the brightness temperature of 10.8 $\mu$m minus that of 12.0 $\mu$m.  Inspection of BTD images found that cirrus clouds had larger absolute temperature difference values than cloud free or low, thick and multi-layered cloud types.  The primary cause is due to the large variation in ice crystal emissivity between 10 $\mu$m and 12 $\mu$m.  Another factor is related to the strong water vapor absorbing constituent in the 10 $\mu$m window region, which dominates in the lower atmosphere.  The resulting emissivity of low, thick, water phased clouds is near unity in the 8 to 13 $\mu$m range, suggesting that the BTD should be close to zero.  Larger BTD values will occur when lower emissivity ice phase clouds are sensed.

7

Inoue's (1987) study area was limited to the tropical ocean dominated by five cloud types, namely cumulus, stratocumulus, cumulonimbus, cirrus and cirrus with lower clouds. Fig. 4 shows the two dimensional threshold scheme, where dense cirrus refers to cirriform clouds with emissivities greater than 0.8. The BTD threshold for identification of low level clouds is set at 1.0 °C, and for high-level clouds it is set at 0.5 °C. The classification derived was verified against Japan Meteorological Satellite Center (JMSC) nephanalysis charts. Results showed that cirrus and cumulus clouds are generally well classified, while very thin cirrus and thin stratocumulus are not. Some cirrus analyzed as dense cirriform cloud lines by JMSC were classified as cumulonimbus by the objective analysis. Because dense cirrus and cumulonimbus clouds share the same 0.5 °C BTD threshold, exact verification would require radar measurements.

## D. OPERATIONAL MODELS

Two operational models are presented which show the state of the art in current automated nephanalysis schemes. Both are interactive in nature, allowing trained meteorologists to adjust and fine tune the analysis. The global model requires significant computer hardware in order to run, and is comprehensive in the data base ingested to
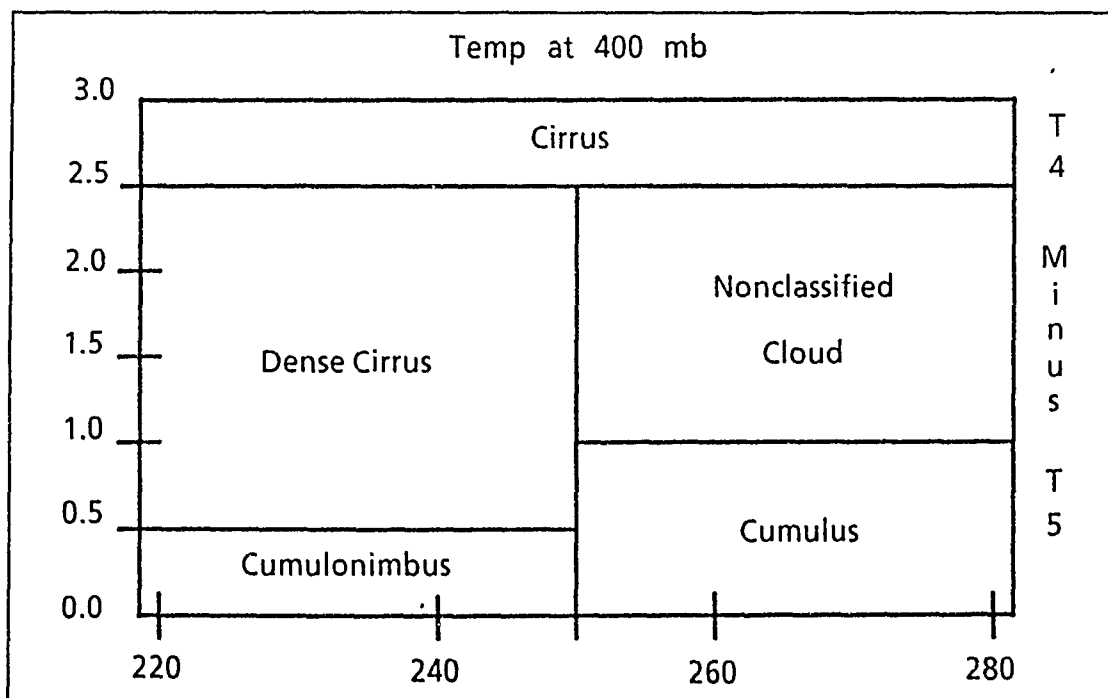


Fig. 4.    Split window technique for cloud classification.    From Inoue (1987), with temperature at 400 mb in K and temperature difference in °C.

8

the model. The global model uses polar orbiting satellite data, while the regional model uses geostationary orbiting satellite data.

1. Global

The Air Force Global Weather Central (AFGWC) automated real-time cloud analysis (RTNEPH) model (Kiess and Cox 1988) is an operational global nephanalysis. Their scheme uses both conventional observations and satellite imagery for determining up to four cloud layers per 46 km resolution polar stereographic grid point. Conventional observations ingested include surface observations, rawinsonde and aircraft pilot reports. Satellite data can be entered from four polar orbiting satellites, accessed from the Satellite Global Data Base (SGDB), using both a visual and infrared channel. A histogram method is employed to form clusters from these channels, which are then classified into ten possible cloud types using a bispectral box type scheme combined with a variance calculated texture parameter. Both visual and infrared data provide brightness values indicating amounts of reflected visual or radiated infrared energy. The determination of cloud cover requires a comparison of sensed values with expected background values, correlated to surface albedo for visual data and surface temperature for the infrared.

The AFGWC RTNEPH model has been operational since August 1983. The analyses is computer intensive, having separate processors for satellite, conventional, merge and bogus processes. The bogus processor enables manual modifications by trained meteorologists to correct deficiencies in the automated analysis. Ten cloud types are distinguished, with conventional reports overriding the satellite analysis when available data overlaps. Problems with the scheme include under interpreting low clouds, coastline bias, snow, ice misinterpretation, high terrain bias and missing small scale clouds. Future upgrades to the analysis include better surface temperature models, incorporation of Special Sensor Microwave Imagery (SSM, I) data, increasing satellite horizontal resolution from 6 km to 3 km, multispectral techniques using NOAA AVHRR, and increasing the models grid resolution from 46 km to 23 km.

2. Regional

The Japanese Meteorological Administration (JMA) produces a nephanalysis product designed to represent horizontal and vertical cloud distribution. The Satellite Cloud Information Chart (SCIC) is constructed by using Geostationary Meteorological Satellite (GMS) infrared data. Two SCIC products of different resolution are produced, one localized for Japan and the other encompassing the whole Far East. Cloud distribution is based on black body temperature contours showing clear, low, middle, high and

highest cloud areas. The categorization is based on observed and analyzed surface, 700 mb, 400 mb and highest level temperatures which act as threshold values. The model is interactive, with manual interpretations added to the localized product to include intensity, development of a system, spatial change of cloud areas, cloud type, cloud pattern and movement.

# III.  AUTOMATED CLOUD ANALYSIS MODEL

An automated interactive multispectral nephanalysis model is presented based on many of the concepts discussed. The Naval Postgraduate School (NPS) model produces a detailed regional cloud analysis, which can be applied in a global context. A systematic method for determining the threshold criteria used in the model for discriminating between cloud types is explored. The generalization of parameters will allow for accurate cloud classifications in different latitudinal regions experiencing a variety of solar elevation angles. This will enable the model to be run efficiently for any region of interest around the world.

## A.  SENSOR SPECIFICATIONS

The following channel characteristics for the AVHRR sensor indicate the potential for a multispectral cloud typing scheme. The NOAA AVHRR is a scanning radiometer that simultaneously senses reflected sunlight and emitted thermal infrared energy in the five channels, or window regions listed in Table 1. Some AVHRR instruments do not contain channel 5, with NOAA-10 being the last operational satellite without the extra infrared channel. The NOAA satellites fly the sensor in a sun synchronous orbit at 850 km altitude, with an orbital inclination of 99° and period of 102 min. The sensor provides global coverage and is available to a wide range of user groups. The instrument scan width is 2800 km, with each scanline comprised of 2048 pixels, represented as 10 bit digital counts. The subsatellite point resolution is 1.1 km for all channels. Calibration coefficients are included for all channels in each scan line.

Table 1.  TIROS-N AVHRR CHANNEL CHARACTERISTICS:  Wavelength in μm.

| Satellite | Channel 1 | Channel 2 | Channel 3 | Channel 4 | Channel 5 |
|-----------|-----------|-----------|-----------|-----------|-----------|
| NOAA-9 | 0.58-0.68 | 0.725-1.10 | 3.55-3.93 | 10.3-11.3 | 11.5-12.5 |
| NOAA-10 | 0.58-0.68 | 0.725-1.10 | 3.55-3.93 | 10.5-11.5 | none |
| NOAA-11 | 0.58-0.68 | 0.725-1.10 | 3.55-3.93 | 10.3-11.3 | 11.5-12.5 |

### 1. Visual

Channel 1 senses reflected solar radiation in the 0.58 - 0.68 $\mu$m electromagnetic band corresponding to the colors yellow, orange and red. This band, using the longer wavelengths of the visual spectrum, is more transparent to visible light passing through the atmosphere, thin stratus and cirrus clouds. The channel provides a daytime cloud mapping capability by its ability to determine surface albedos. Given a digital radiometer count ($X$), and assuming the albedo is a linear function, the percent albedo ($A$) of the target is given by

$$A = GX + I,$$

where $G$ and $I$ are the gain and intercept of the visible channel. The albedo then can be normalized to an overhead sun by dividing by the cosine of the solar zenith angle, if the cloud acts as an isentropic reflector.

### 2. Near Infrared

Channel 2 senses near infrared reflected solar radiation from 0.725 - 1.10 $\mu$m. This channel is used for land-water delineation as reflectance of terrestrial surfaces (vegetation) is higher than in channel 1. Land backgrounds that appear dark in the visible imagery appear brighter in the near-infrared imagery. Cloud reflectance is similar for both channels, but it is significantly less in channel 2 for ice and snow surfaces. It is very useful in constructing an overview of the total satellite pass and the regional subscene, as it shows terrestrial landmarks used for accurate navigation.

### 3. Infrared

Channel 4 senses 10.3 - 11.3 $\mu$m infrared emitted terrestrial radiation, enabling measurements of surface and cloud top temperatures. A single measurement of radiant flux and a knowledge of the surfaces emissivity is sufficient to define the temperature. Even though channel 4 is an atmospheric window region, radiation emitted at these wavelengths is noticeably affected by water vapor. Land surface temperatures and cloud top temperatures can be measured with a two K accuracy, during both day and night. Channel 5 senses 11.5 - 12.5 $\mu$m emitted thermal radiation and has the same characteristics as channel 4, except that channel 5 radiation is even more sensitive to atmospheric water vapor. Corresponding measured brightness temperatures from both channels are similar for clear, cold atmospheres since they are usually quite dry. But due to attenuation by atmospheric water vapor, channel 5 brightness temperatures are as much as

3 % lower than their corresponding channel 4 temperatures when measured for moist atmospheres.

## B.  MULTISPECTRAL ALGORITHM

The NPS model classifies eleven cloud types (Table 2) using a multispectral approach employing high resolution imagery.  Data are obtained from NOAA polar orbiting satellites carrying the five channel AVHRR imaging sensor.  The sunsynchronous orbit of the satellite enables global analyses to be made, while the additional channels on the sensor allow for a detailed multispectral approach in typing clouds.  The model algorithm uses a three dimensional box scheme (Fig. 5) to produce the automated nephanalysis.  A statistical texture routine is used to distinguish between similar stratiform and cumuliform cloud types.  Thresholds required for the cloud type analysis include five 10.8 $\mu$m infrared temperatures, three 0.63 $\mu$m albedos and one infrared temperature difference between 10.8 and 12.0 $\mu$m.

Table 2.  CLOUD TYPES DISCRIMINATED IN NPS MODEL

| Step # | Cloud Name | Symbol | Color |
|--------|------------|--------|-------|
| 1 | Stratus | St | Brown |
| 2 | Stratocumulus | Sc | Red |
| 3 | Cumulus | Cu | Orange |
| 4 | Altocumulus | Ac | Yellow |
| 5 | Altostratus | As | Lt Green |
| 6 | Cumulus Congestus | Cu C | Dk Green |
| 7 | Cirrus | Ci | Slate |
| 8 | Cirrocumulus | Cc | Blue |
| 9 | Cirrostratus | Cs | Navy |
| 10 | Nimbostratus | Ns | Magenta |
| 11 | Cumulonimbus | Cb | Purple |

The NPS model requires three processed AVHRR satellite images of the subscene being analyzed in order to run.  A channel 1 reflectance scaled by solar zenith angle is required for pixel comparison with the albedo threshold values set in the model.  A channel 4 infrared brightness temperature, calibrated in K, is needed for determining terrestrial surfaces and cloud top temperatures for comparison with the infrared thresh-

13

CH45

Ci

Cs

Cs

Cc

Cb

Cs

Cb

Cs

Cb

Cs

IR 5

Cs

Ns

Ci

Cc

Ns

Cu c

Cs

As

Cs

As

Cu c

As

Sc

Cu

St

Cu

Sc

Cu

St

Cu

CH45

IR 4

IR 3

IR 2

IR 1

ALB 1     ALB 2     ALB3
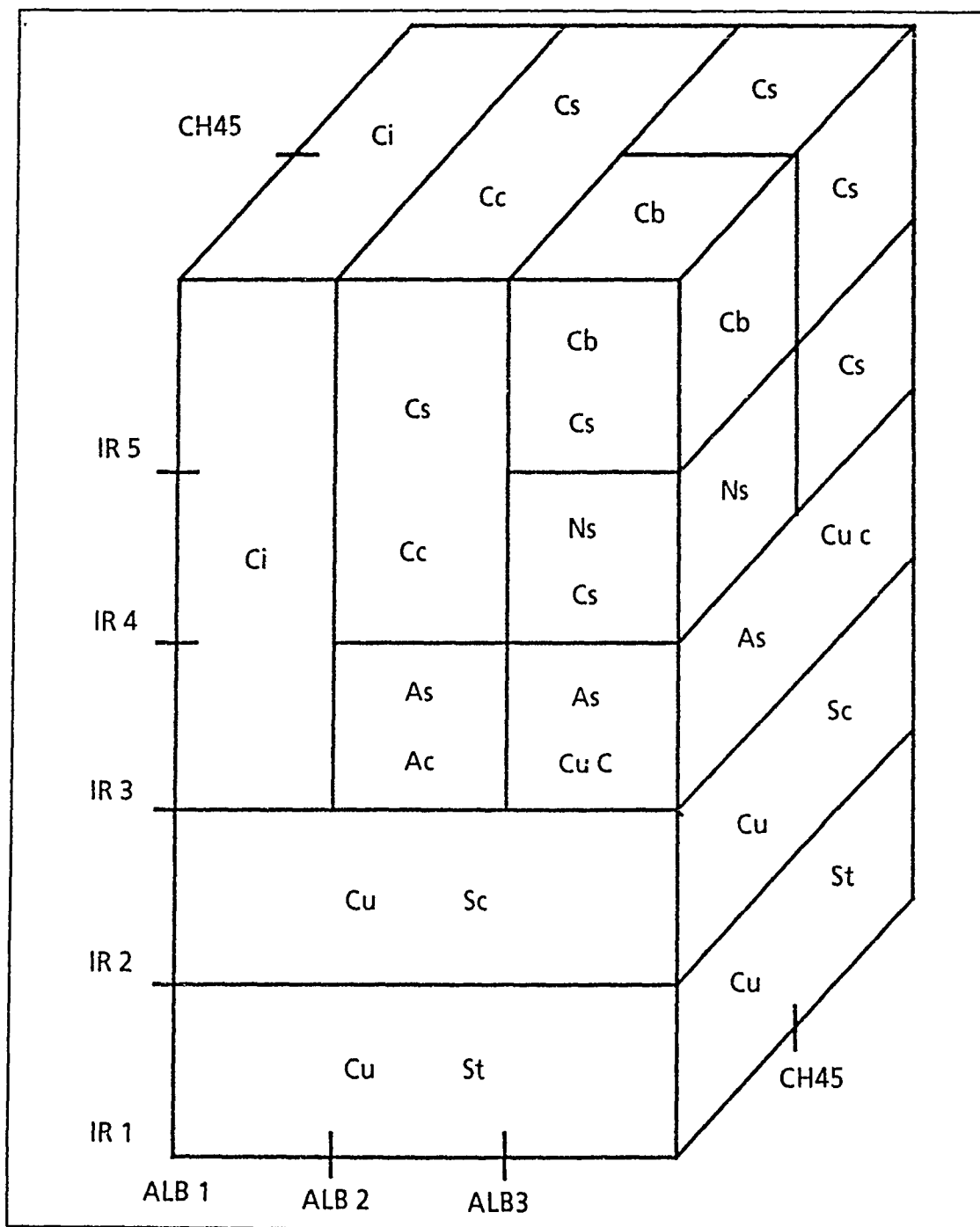
Fig. 5.    Automated multispectral nephanalysis NPS model. Thresholds for albedo are in %, temperature in K and temperature difference in °C.

old values set in the model. The third image required of the subscene is a channel 4 and channel 5 brightness temperature difference, calibrated in °C, for comparison with the

14

model threshold value. The lower the temperature difference the thicker the cloud type being sensed.

## C. CLOUD BRIGHTNESS

Different cloud types have different brightness signatures in the visible and infrared spectrum. Satellite imagery detects cloud cover based on the contrast between the clouds and their background. The contrast is produced in terms of reflectance differences for visual wavelengths, and brightness temperatures for infrared wavelengths. Daytime satellite radiance measurements consist of radiance from thermal emission of the viewed surface and radiance due to solar reflection. If the transmissivity between the satellite and the viewing surface is 1.0, the amount of radiance from thermal emission reaching the satellite is determined by the viewed surface's emissivity. The amount of reflected solar radiance reaching the satellite is determined by the incident solar radiance and the reflectance of the viewed surface. Incident solar radiance is weighted by the cosine of the solar zenith angle, while the directional reflectance is a function of solar zenith angle, the satellite zenith angle and the horizontal angle between them. Anisotropic reflectance arises due to the directional dependence of the scattering mechanisms.

### 1. Albedo

Albedo signatures differ for land, ocean and the various cloud types. Land and ocean surfaces are characterized by relatively low albedos, except in regions of sun glint over the ocean. Clouds show higher albedos, the value of which increases as a function of optical depth, water phase and particle size. This is useful in distinguishing between cloudy and clear areas given a knowledge of terrestrial brightness values. The reflected radiance in the visible spectrum is dependent on solar zenith angle, as lower sun elevation angles reduce the solar radiance per unit area reaching the cloud top. It also depends on the amount of solar radiance reflected by the viewed cloud back toward the satellite. The assumption that clouds are isentropic reflectors is made in an attempt to standardize reflected solar radiances for different solar zenith angles. This is accomplished by dividing the calculated albedos by the cosine of the solar zenith angle.

Albedo thresholds represent the boundaries between terrestrial surfaces and clouds, as well as low emissivity ice phased clouds, high emissivity ice phase clouds and thick water phase clouds. Table 3 states the generalized values used in the NPS model, in an attempt to portray average albedo characteristics. In an operational setting, the model routine does allow manual modification of the values, enabling one to fine tune

15

the analysis for localized areas. Values near the low end of the threshold range would be appropriate for winter, high solar zenith angle or ocean surface subscenes. Values toward the high end of the range reflect conditions found during summer, low solar zenith angle or bright terrestrial surface subscenes. The reflectance in channel 1 images is scaled between 0 and 255, allowing the albedo at each pixel to be calculated by

$$ALB = \left( \frac{1}{255.0} \right) \left( \frac{CNT}{\cos \theta} \right),$$

where $ALB$ is the albedo in percent, $CNT$ is the raw grey shade brightness value at the pixel and $\theta$ is the solar zenith angle.

Table 3. ALBEDO THRESHOLDS IN NPS MODEL: Generalized values for analysis.

| Threshold | ALB 1 | ALB 2 | ALB 3 |
|---|---|---|---|
| Value (%) | 0.08 | 0.20 | 0.45 |
| Range (%) | 0.05 - 0.15 | 0.15 - 0.35 | 0.35 - 0.55 |

## 2. Temperature

Infrared temperature signatures provide low, middle and high cloud type differentiation, as well as cloud versus no-cloud determination, when the surface and vertical temperature profile are known. The infrared brightness temperature provides the temperature, through calibration coefficients, of the surface or cloud top. If the vertical temperature profile of the atmosphere is known, one can determine the height of the cloud tops. A blackbody cloud will follow Planck's function, which relates the emitted monochromatic intensity with the wavenumber and temperature of the emitting surface. The generalized heights at which the temperature threshold values are obtained is shown in Table 4. Cloud top heights are generally found at higher altitudes in tropical than in polar regions. The range of threshold heights listed serves as a reference for localized analyses from the tropics (high) to the poles (low).

16

Table 4. TEMPERATURE THRESHOLD HEIGHTS IN NPS MODEL: Generalized values for analysis.

| Threshold | IR 1 | IR 2 | IR 3 | IR 4 | IR 5 |
|---|---|---|---|---|---|
| Value (m) | Sfc | 1500 | 2500 | 6500 | 7500 |
| Range (m) | Sfc | 1-2 km | 2-3 km | 6-7 km | 7-8 km |

A knowledge of the atmospheric temperature structure and the height at which different cloud types are normally found provides the needed inputs for the NPS model temperature thresholds. Both rawinsonde and automated gridded temperature data are used to obtain the average subscene vertical temperature structure. Care must be taken in determining an accurate portrayal of the temperature profile, as rawinsondes provide a point measurement while numerical gridded data provide a volume measurement. The channel 4 image used in the analysis is bounded by 312 K on the warm end and 185 K on the cool end. A pixel temperature, in K, can be computed through a calibration process of converting brightness values to temperature by

$$TEMP = \left( \frac{CNT}{-2.008} \right) + 312.0.$$

3. Temperature Difference

The infrared temperature difference threshold is set to distinguish between high emissivity ice phased clouds and thick, multilayered water phased clouds. This is needed because the distinction can't be done accurately from the cloud types albedo characteristics alone. The generalized threshold value used in the NPS model is 0.5 °C, obtained from Inoue's (1987) work in distinguishing dense cirrus clouds from cumulonimbus and nimbostratus clouds. The operational model does allow this value to be adjusted in order to tailor it for localized conditions. The channel 5 brightness values are subtracted from the channel 4 brightness values, with the resulting split window image scaled between -20 and 20 °C. The temperature difference in °C can be calculated by

$$CH45 = \left( \frac{CNT}{6.375} \right) - 20.0.$$

17

## D.  CLOUD TEXTURE

Cloud texture is relatively easy to visualize in a qualitative sense, but quantitative interpretations of this important image characteristic are more elusive.  The model pursues a statistical rather than structural interpretation of texture, measuring local variations in the visual image albedos for the sub-array in question.  The standard deviation for each sub-array density value is then calculated, providing a simple and standard measure of the local density variation.  This measure is intuitively acceptable for expressing quantitative assessments of roughness of a surface (Harris and Barrett, 1978).  It is expressed by the standard formula

$$\sigma = \left[ \sum_{i=1}^{n} \sum_{j=1}^{n} (x_{ij} - \bar{x})^2 / n^2 - 1 \right]^{1/2} ,$$

where n is the number of pixels per row and column in the sub-array, $x_{ij}$ is the density value of each pixel and $\bar{x}$ is the mean value of pixels in the sub-array.

The NPS model provides a textural field of view equal to 2.2 km by setting n equal to 2.  This allows adequate resolution in defining small cumulus clouds.  Under this analysis, clouds with a uniform or stratiform texture will have low standard deviation values.  Table 5 lists the cloud types discriminated by the statistical texture approach applied to the visual albedos with their corresponding threshold values.

Table 5.  STATISTICAL TEXTURE ANALYSIS

| Test | Cloud Type | Threshold |
|------|------------|-----------|
| 1 | Cirrostratus | < 0.02 |
| 1 | Cirrocumulus | ≥ 0.02 |
| 2 | Altostratus | < 0.03 |
| 2 | Cumulus Congestus | ≥ 0.03 |
| 3 | Altostratus | < 0.02 |
| 3 | Altocumulus | ≥ 0.02 |
| 4 | Stratocumulus | < 0.04 |
| 4 | Cumulus | ≥ 0.04 |
| 5 | Stratus | < 0.05 |
| 5 | Cumulus | ≥ 0.05 |

# IV. DATA ANALYSIS

Four case studies were chosen for the validation process of the NPS cloud analysis model (Table 6). The rationale used in choosing a case was based on its geographic position, solar zenith angle, availability of supporting data and presence of interesting cloud features. The goal of the cloud analysis is to produce a valid cloud classification anywhere on earth, and thus it requires subscenes from different latitudes and longitudes for a meaningful validation. Subscenes with different solar zenith angles were chosen in an attempt to see how the sun's elevation angle affects the cloud analysis. Supporting data are needed in the form of rawinsondes and numerical gridded data fields for determining the atmospheric vertical temperature structure. Finally, each subscene requires the presence of a large variety of cloud types, including those types which present the greatest challenge to automated classification schemes.

Table 6. CASE STUDIES FOR VALIDATION: Ascending satellite node.

| Case | Date | Time (UTC) | Zenith L (deg) | Center (deg) | |
|------|------|------------|----------------|--------------|---|
| | | | | Lat. (N) | Lon. (W) |
| 1 | 13 DEC 88 | 1809 | 31.3 | 20 | 69 |
| 2 | 17 JAN 88 | 2256 | 54.6 | 34 | 119 |
| 3 | 13 DEC 88 | 1809 | 38.5 | 34 | 74 |
| 4 | 14 DEC 88 | 1758 | 46.4 | 42 | 70 |

One subscene from the tropics, two from the subtropics and one from the mid-latitudes were chosen. The two subtropical subscenes differ in that one is along the western United States and characterized by a high solar zenith angle, while the other is along the eastern United States with a relatively low solar zenith angle. The supporting data were obtained from the January 1988 (JAN88) storm, which passed over the central California coast on the 17th, and from the Experiment on Rapidly Intensifying Cyclones over the Atlantic (ERICA) for Intensive Observation Period (IOP) 2. Effort was taken to incorporate as many different cloud types as possible in each subscene. Instances of thin cirrus near land, cumulonimbus or nimbostratus clouds embedded in thick cirrostratus clouds and low clouds over cold land were selected, as they have posed

19

problems in other automated classifications (Reynolds and Vonder Haar 1976; Liljas 1982).

## A. CASE 1

The tropical subscene chosen for analysis is located over the northern Caribbean Sea and eastern Greater Antilles. Fig. 6a shows a channel 2 image of the area, with latitude and longitude given for geographic orientation. The image depicts the island land surfaces clearly and provides a general overview of the cloud coverage and patterns. The cloud types of interest include thin cirrus to the north of the Dominican Republic and Puerto Rico, as well as the formation of convective clouds over the higher island terrain. Fig. 6b portrays the channel 1 image, Fig. 6c is the channel 4 image and Fig. 6d represents the channel 4-5 temperature difference image for the subscene. The thin cirrus is barely discernable in the visual image, but is readily apparent in the infrared. The low clouds and developing cumulus over the land areas are identifiable from both the visual and infrared imagery.

The supporting data used in the analysis were two rawinsondes and the NMC spectral analysis gridded data. One rawinsonde is located at Santo Domingo (SDQ:78486), at latitude 18°28'N and 69°53'W. The other rawinsonde is from San Juan (JSJ:78526), at latitude 18°26'N and 66°00'W. Both temperature soundings used in the analysis were taken at 1200 UTC on December 13, 1988 and are shown in Fig. 7a as a linear temperature versus height plot. The spectral gridded analysis was used to create a vertical temperature profile at the center point of the subscene, located at 20°0'N and 68°30'W. Fig. 7b is a graphical representation of the height and temperature versus pressure for the location. The three temperature profiles are within 1 K throughout the vertical, with the greatest temperature differences near the surface. The rawinsondes show a pronounced inversion between 2500 and 3000 m, while the spectral profile smooths over this feature.

## B. CASE 2

This subscene is bounded by latitudes 31°N to 36°N, and by longitudes 122°W to 116°W, falling into a subtropical categorization along the western United States coast. Fig. 8a provides a channel 2 image of the region, showing the extratropical cyclone center moving over Point Conception, California. The storm presents a wide variety of cloud types for analysis. The cold frontal region consists of convective clouds embedded in various densities of cirrus clouds and thick stratiform clouds. Low stratus and cumulus clouds are present in the cold air to the west through south of the low center

20

with middle clouds near the center of the low. Fig. 8b, Fig. 8c and Fig. 8d show the channel 1, channel 4 and channel 4-5 difference images, respectively.

Two rawinsondes and a spectral gridded data temperature profile were obtained from 1200 UTC data on January 17, 1988. The first rawinsonde, from Vandenburg AFB (VBG:72393), is located at 34°43'N and 120°34'W, while the second, from San Diego's Montgomery Field (MYF:72290), is located at 32°49'N and 117°08'W. A temperature
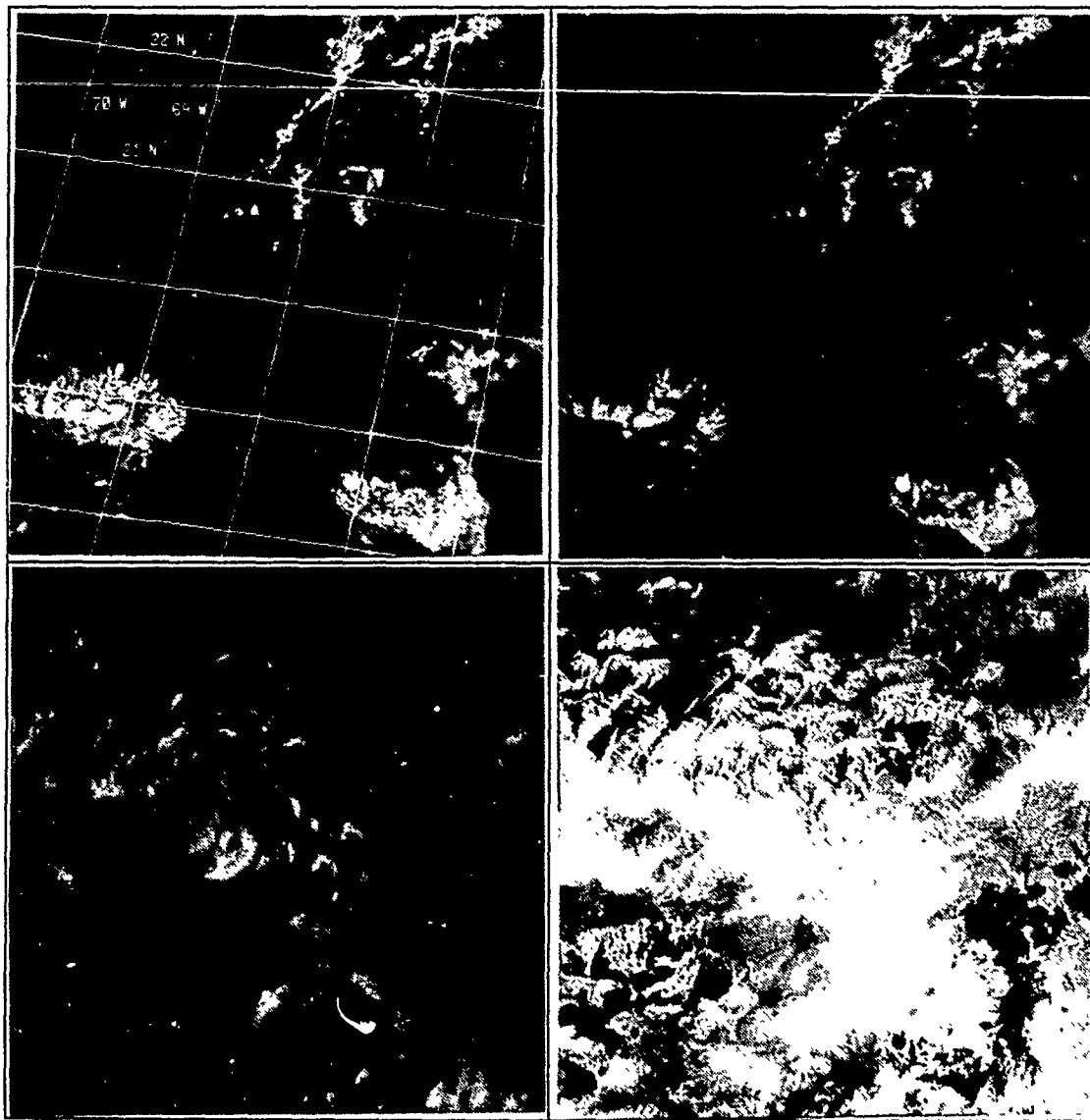


Fig. 6. Case 1 satellite imagery. NOAA-11 AVHRR at 1809 UTC 13 December 1988. Fig. 6a (upper left) is channel 2, Fig. 6b (upper right) is channel 1 scaled by solar zenith angle, Fig. 6c (lower left) is channel 4 and Fig. 6d (lower right) is enhanced channel 4-5 difference.

21
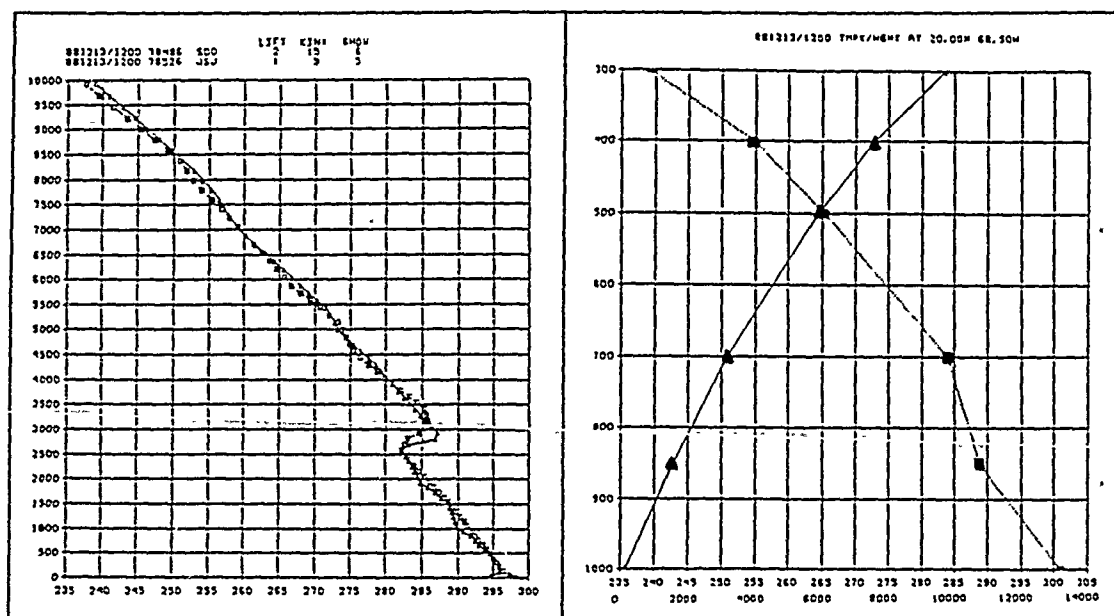
Fig. 7. Case 1 temperature profiles. 1200 UTC 13 December 1988. Fig. 7a (left) shows SDQ (triangle) and JSJ (square) rawinsonde soundings as linear height (m) and temperature (K) plot, Fig. 7b (right) shows spectral gridded profile as linear pressure versus temperature (square) and linear pressure versus height (triangle) plot.

profile at 33°30′N and 118°32′W, the center point of the subscene, was created using the spectral gridded data analysis at 1200 UTC on January 17, 1988. Fig. 9a and Fig. 9b show the rawinsonde and gridded profiles, respectively. The three vertical temperature profiles are within 2 K up to 6000 m, with departures of approximately 5 K found above. The spectral profile appears slightly colder in the lower levels than the rawinsondes.

## C. CASE 3

An intensifying shortwave moving off the eastern United States seaboard was chosen for this subtropical subscene. Fig. 10a shows the region centered between the North Carolina coast and eastern Sargasso Sea, with the channel 2 imagery portraying the general synoptic cloud pattern. Stratified middle and high level clouds are present throughout the disturbance, with a convective region over in the eastern portion. Thin cirrus and low clouds are found in the west sector of the shortwave. Fig. 10b shows the channel 1 image, Fig. 10c is the channel 4 image, with the channel 4-5 difference image depicted in Fig. 10d.

The vertical temperature profile was obtained from a rawinsonde and two dropwinsondes, as well as a spectral gridded analysis field. The Cape Hatteras (HAT:72304) rawinsonde site, located at 35°16′N and 75°33′W, provided a 1200 UTC sounding on December 13, 1988. Two NOAA dropwinsondes were recorded in the area at approximately 1500 UTC, located near 34°N and 71°W. The three profiles are shown as linear plots in Fig. 11a. The center point of the subscene, 34°19′N and 74°20′W, was
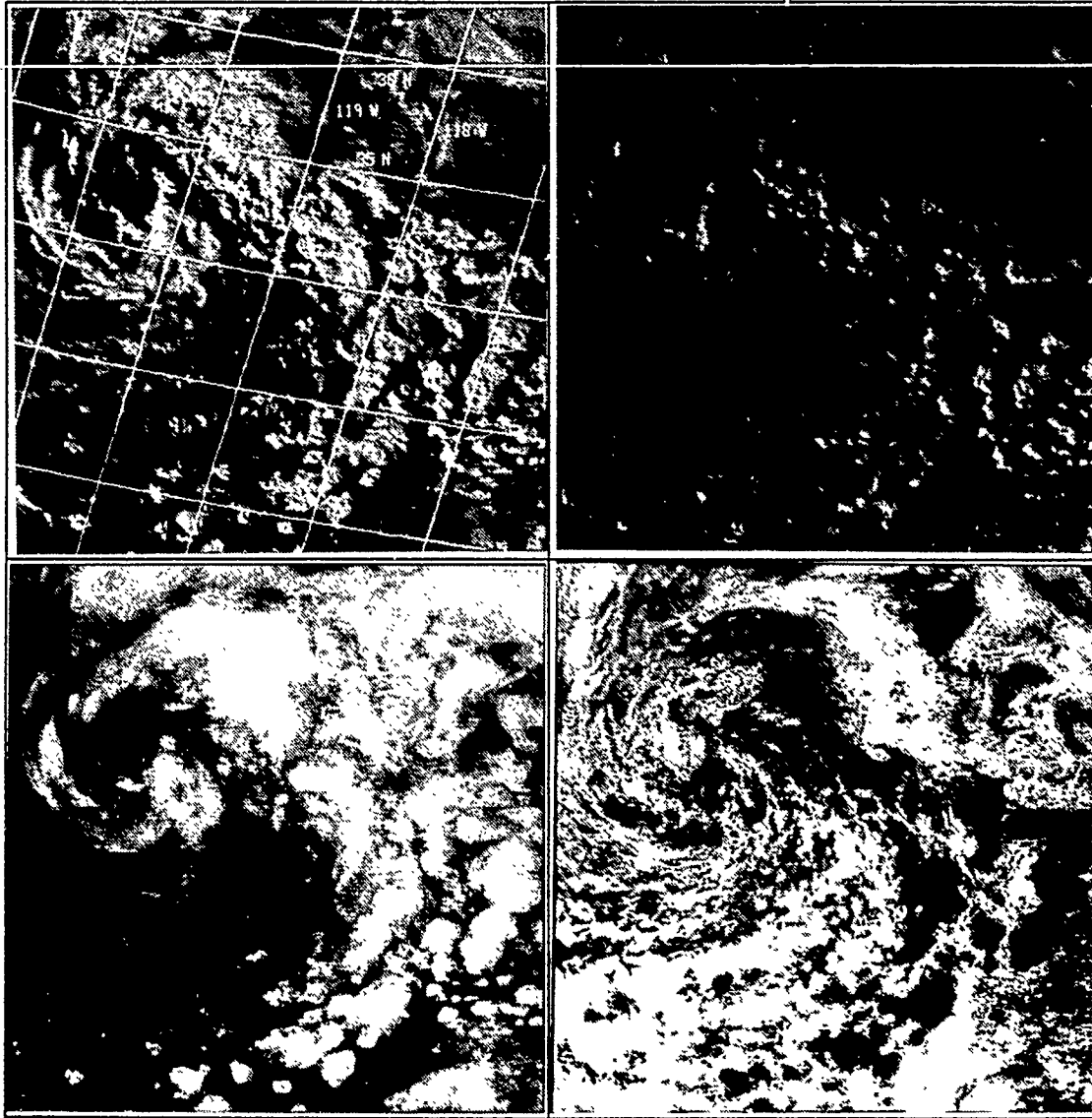


Fig. 8.    Case 2 satellite imagery.    NOAA-9 AVHRR at 2256 UTC 17 January 1988.  Fig. 8a is channel 2, Fig. 8b is channel 1 scaled by solar zenith angle, Fig. 8c is channel 4 and Fig. 8d is enhanced channel 4-5 difference.

23
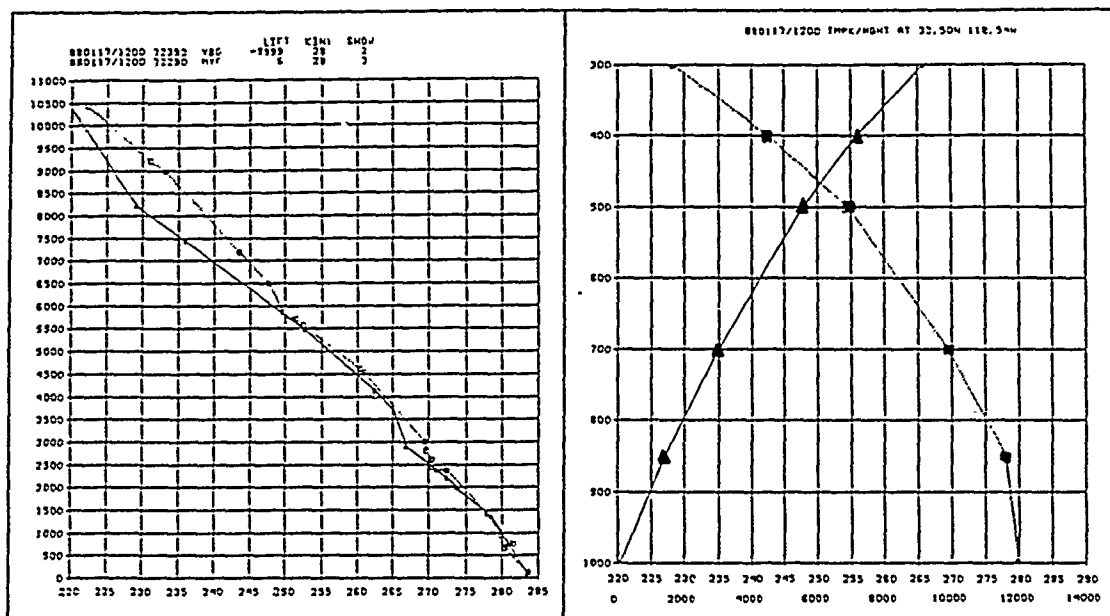
Fig. 9. Case 2 temperature profiles. 1200 UTC 17 January 1988. Fig. 9a shows VBG (triangle) and MYF (triangle) rawinsonde soundings as linear height (m) and temperature (K) plot, Fig. 9b shows spectral gridded profile as linear pressure versus temperature (square) and linear pressure versus height (triangle) plot.

chosen to construct a vertical temperature profile from the spectral gridded analysis at 1200 UTC on December 13, 1988. Fig. 11b shows the resulting linear plot. A greater variation in the four vertical temperature profiles is found for this case, showing a consistent 5 K spread among them with height.

## D. CASE 4

The final case study is located in the mid-latitudes, with the subscene encompassing southern New England and eastern Georges Bank. The channel 2 image in Fig. 12a, shows the land areas, with latitude and longitude lines drawn for reference. The channel 1, channel 4 and channel 4-5 difference images are presented in Fig. 12b, Fig. 12c and Fig. 12d, respectively. Low clouds over the coastal region and a band of high clouds further to the east can be discerned from the infrared image. The visual image distinguishes the land surface from overlying low clouds and thin cirrus clouds. A variety of cloud types are present, however the subscene does lack convective and stratiform precipitating cloud types.

Data used in determining the representative vertical temperature structure include three rawinsonde sites and spectral gridded analysis, all from 1200 UTC on December

24

14, 1988. One rawinsonde is from Albany (ALB:72518), located at 42°45′N and 73°48′W, another at Chatham (CHH:74494), located at 41°40′N and 69°58′W, and the third is from Portland (PWM:72606), located at 43°39′N and 70°19′W. A profile was constructed from the spectral gridded data analysis for the center point of the subscene at 42°01′N and 70°26′W. Fig. 13a and Fig. 13b show the rawinsonde and gridded pro-



Fig. 10.    Case 3 satellite imagery.   NOAA-11 AVHRR at 1809 UTC 13 December 1988.   Fig. 10a is channel 2, Fig. 10b is channel 1 scaled by solar zenith angle, Fig. 10c is channel 4 and Fig. 10d is enhanced channel 4-5 difference.

25

Fig. 11. Case 3 temperature profiles. 1200 UTC 13 December 1988. Fig. 11a shows HAT (triangle) rawinsonde and NC06 (square), NC08 (circle) dropwinsondes as linear height (m) and temperature (K) plot, Fig. 11b shows spectral gridded profile as linear pressure versus temperature (square) and linear pressure versus height (triangle) plot.

files, respectively. A 7 K spread among the four temperature profiles exists from the surface up to approximately 2000 m, decreasing to a 3 K spread above this level.

E. EVALUATION PROCEDURE

The evaluation of an automated cloud classification product requires a form of ground truth for comparison. Two methods are available for this procedure, and both have been used in previous cloud classification research. One method is to use surface observations of clouds over the available reporting stations in the subscene (Allen 1987). The other method is to use an expert manual cloud analysis based on the same satellite imagery as used in the automated scheme (Barron 1988). Both of these methods have associated strengths and weaknesses. The decision was made to use two independent manual nephanalyses, produced by experienced meteorologists, for the verification of the NPS automated analysis.

The following reasons were used in choosing this evaluation procedure. A surface weather observer views the base of the clouds, whereas the satellite is viewing the top of the clouds. In the event that multilayered clouds are present, the lower clouds will

26

restrict the identification of the middle and high clouds from the surface vantage point. Since the automated classification is based on satellite imagery, consistency dictates that the verification also be based from a satellite perspective. The surface observer is also limited by field of view, and can only distinguish clouds accurately within an approximate radius of 50 km from the station. The great distance between observing sites and data sparse regions around the earth, especially over the oceans, makes an indepth ver-
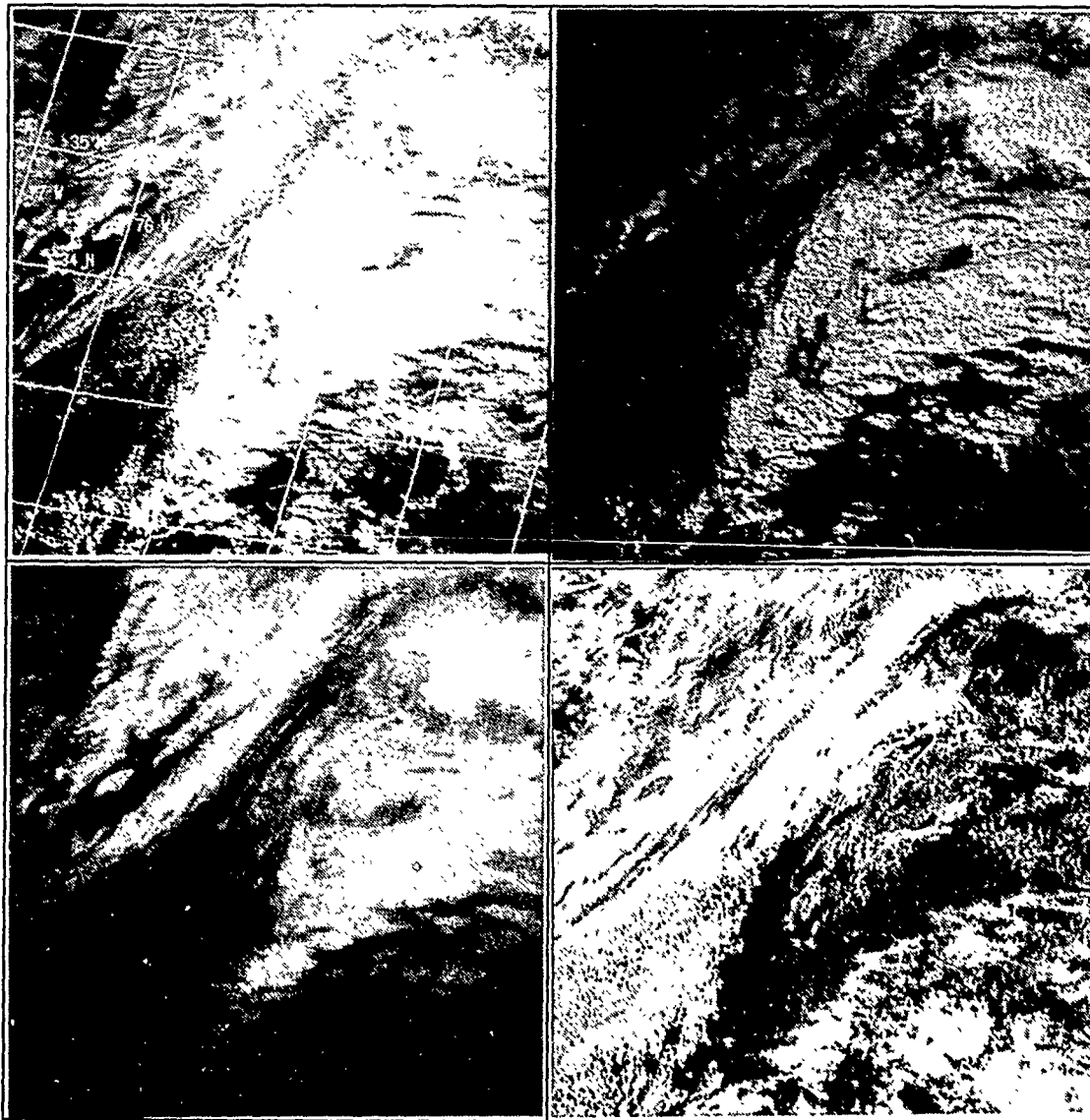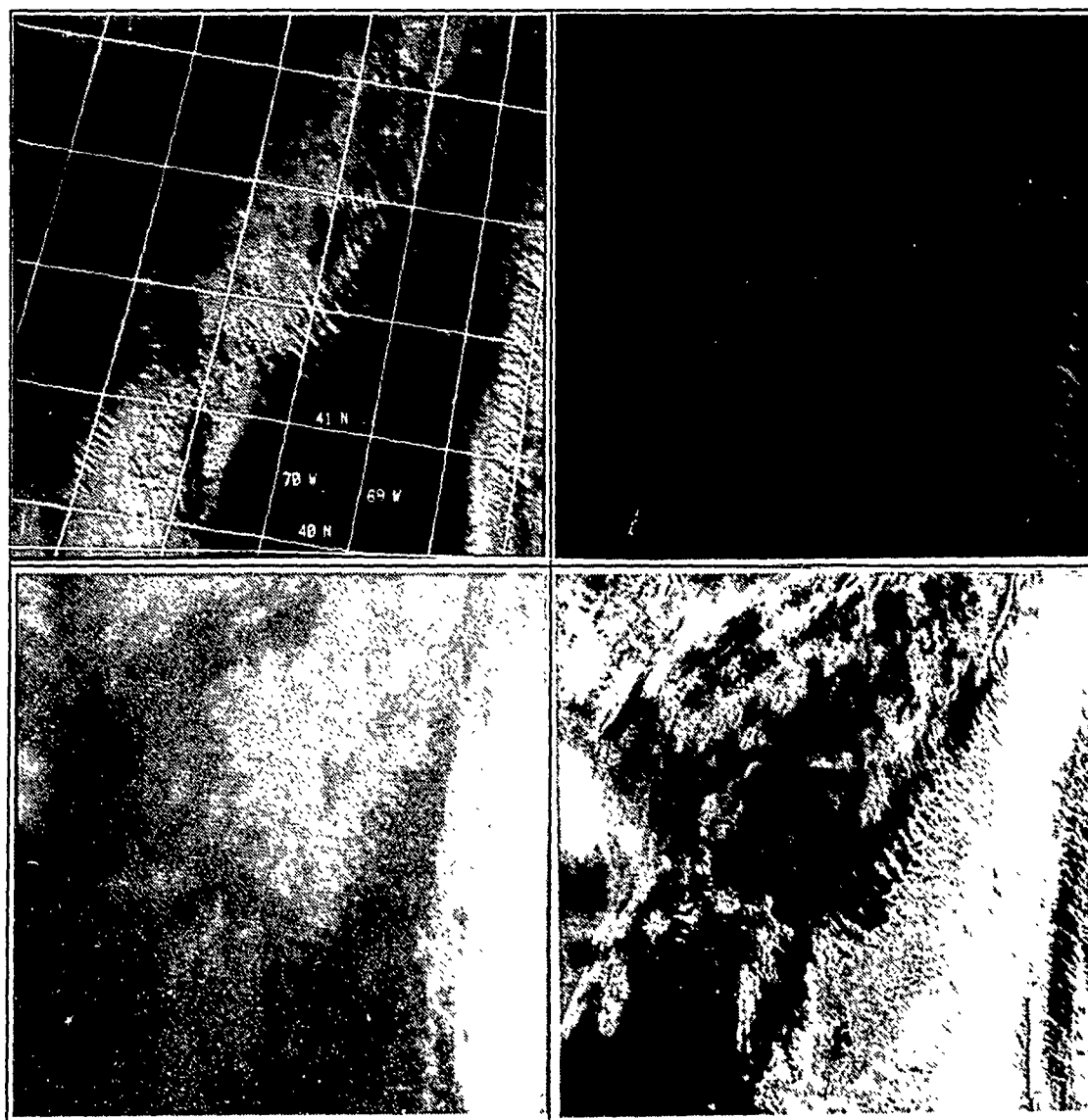


Fig. 12. Case 4 satellite imagery. NOAA-11 AVHRR at 1758 UTC 14 December 1988. Fig. 12a is channel 2, Fig. 12b is channel 1 scaled by solar zenith angle, Fig. 12c is channel 4 and Fig. 12d is enhanced channel 4-5 difference.
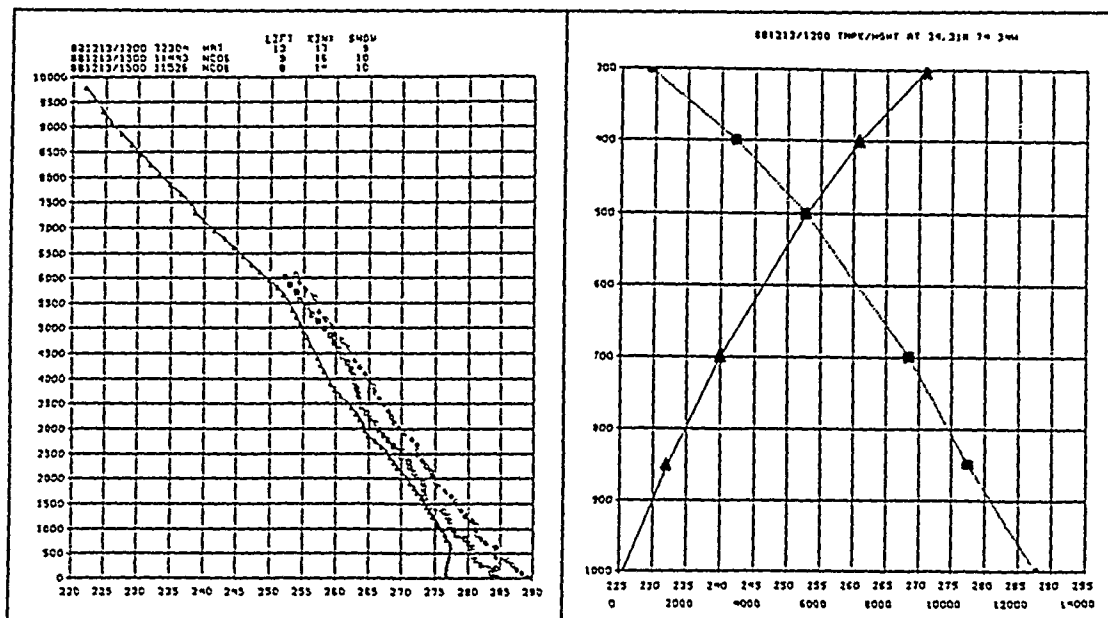
27
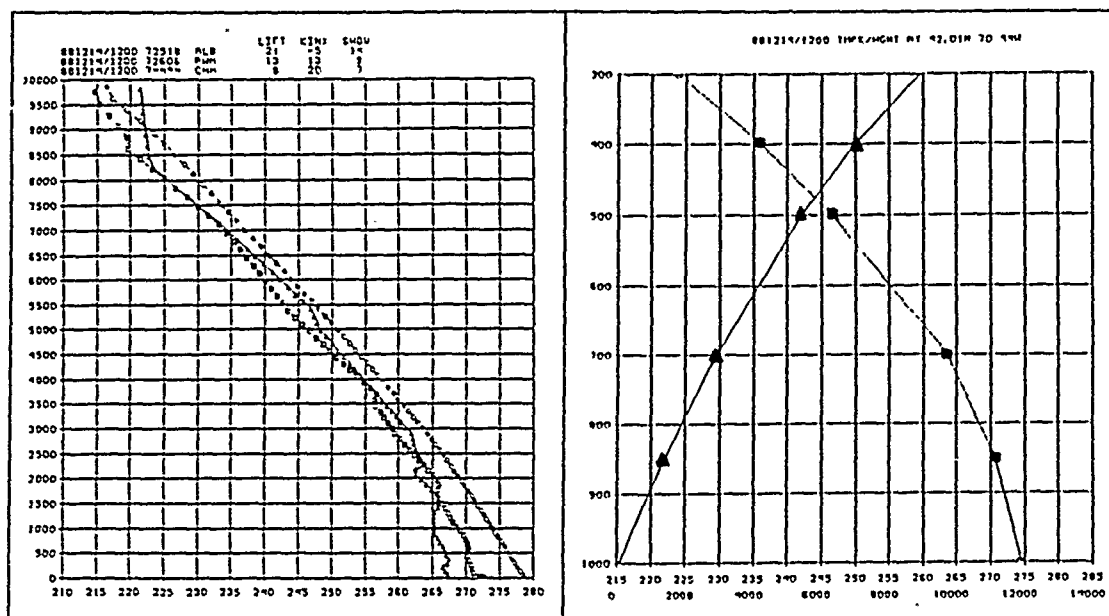
Fig. 13. Case 4 temperature profiles. 1200 UTC 14 December 1988. Fig. 13a shows ALB (triangle), PWM (square) and CHII (circle) as linear height (m) and temperature (K) plot, Fig. 13b shows spectral gridded profile as linear pressure versus temperature (square) and linear pressure versus height (triangle) plot.

ification from surface observations alone virtually impossible. Manual satellite cloud analyses can be made globally with the same spatial resolution as the imaging sensor, and thus offer greater flexibility in choosing a subscene for analysis.

The manual analyst has the advantage of using surface data, upper air data and the same satellite data used by the automated scheme in making the verification decisions. Two independent manual analyses were made for each subscene in an effort to reduce any bias from being introduced. Professors Carlyle H. Wash and Forrest R. Williams, Department of Meteorology, Naval Postgraduate School, provided their expertise in this undertaking. Classifications were produced by placing an eight by eight grid overlay on each of the 512 X 512 visual and infrared images of the subscene. The available rawinsonde, dropwinsonde, numerical spectral gridded analysis and surface observations were also provided for their use.

The dominant cloud types within each box formed by the overlying grid were identified and located using its x, y coordinate position (pixel) in the image. A consensus cloud type was determined from the two independent manual analyses at each pixel location for which there was agreement. Cases of disagreement between the two manual analysts were not used in the evaluation. The consensus results were then compared to

28

the same pixel locations within the automated classification image for a one to one comparison. Since the NPS model resolution is degraded to 256 X 256 by the statistical textural analysis, agreement between model and manual classification is given a 1 pixel tolerance during the comparisons.

## F.  TEMPERATURE THRESHOLDS

The NPS model requires five temperature thresholds for categorizing cloud types. These threshold values are a function of the vertical temperature structure in the subscene and were determined by averaging the rawinsonde data and spectral gridded data for each case independently. A simple mean calculation was performed, weighting each data set equally. The magnitude of the temperature differences between soundings in each of the individual cases ranges between 1 and 7 K. The average difference is within the sensor and numerical analysis model accuracies.  It should be stressed that rawinsondes are point measurements, while the gridded profiles represent volume averages. By combining the two, a representative mean temperature profile was constructed for each case incorporating the strengths of both point and volume measurements. Table 7 lists the values in K at each of the five threshold heights for each of the four cases discussed.

Table 7.  TEMPERATURE   THRESHOLD   VALUES   FOR   CASE STUDIES:  Average rawinsonde, dropwinsonde and gridded data for each case in K.

| Case | IR1 | IR2 | IR3 | IR4 | IR5 |
|------|-----|-----|-----|-----|-----|
| 1 | 298 | 288 | 282 | 262 | 256 |
| 2 | 285 | 277 | 270 | 247 | 242 |
| 3 | 288 | 275 | 267 | 244 | 237 |
| 4 | 273 | 267 | 263 | 240 | 232 |

# V. EVALUATION RESULTS

The evaluation of the NPS cloud classification model is based on a direct comparison between the automated product and a consensus expert manual cloud classification. Color coded automated cloud classification images were generated for each of the analyzed cases. The automated image consists of a 256 X 256 array of pixels, giving a possible 65,536 points for comparison. Evaluation focuses on approximately 45 pixel locations within each of the four cases, bringing the manual interpretation down to a manageable level. These pixel locations are evenly distributed over the image, and were determined by Dr. Wash during development of his manual nephanalysis. Representative cloud types were chosen that portray the overall cloud types and pattern characteristics for each case.

The results are presented in a tabular format, listing the automated classifications in columns and manual classifications in rows. A number is assigned to each resulting block in the table, indicating occurrences of that particular comparison between automated and manual identification. Blank spaces indicate that no classification was made for that combination of manual and model derived cloud types. Perfect matches lie along the diagonal boxes from upper left to lower right, representing the intersection of the same cloud type columns and rows. Misclassifications lie off the diagonal, and indicate the number of times and nature of each discrepancy. Clear conditions are entered as part of the evaluation to represent the cloud, no cloud classification. Results are shown for the 11 specific cloud types analyzed by the model, and for five general categories, namely clear, low clouds, middle clouds, high clouds and precipitation clouds.

## A. CASE 1

Fig. 14 shows the NPS color enhanced cloud analysis image generated from the generalized threshold scheme. A total of 49 pixel locations were chosen for the verification of this case. The automated cloud analysis can be compared with the AVHRR imagery of the case shown in Fig. 6. The model appears to have captured the dominant cloud types in this tropical subscene well. Thin cirrus (slate) over the ocean and low clouds (red, orange) over the islands are clearly portrayed by the color scheme. Precipitation cloud types are scarce in this particular subscene, as evidenced by the lack of colors magenta and purple in the model cloud analysis.
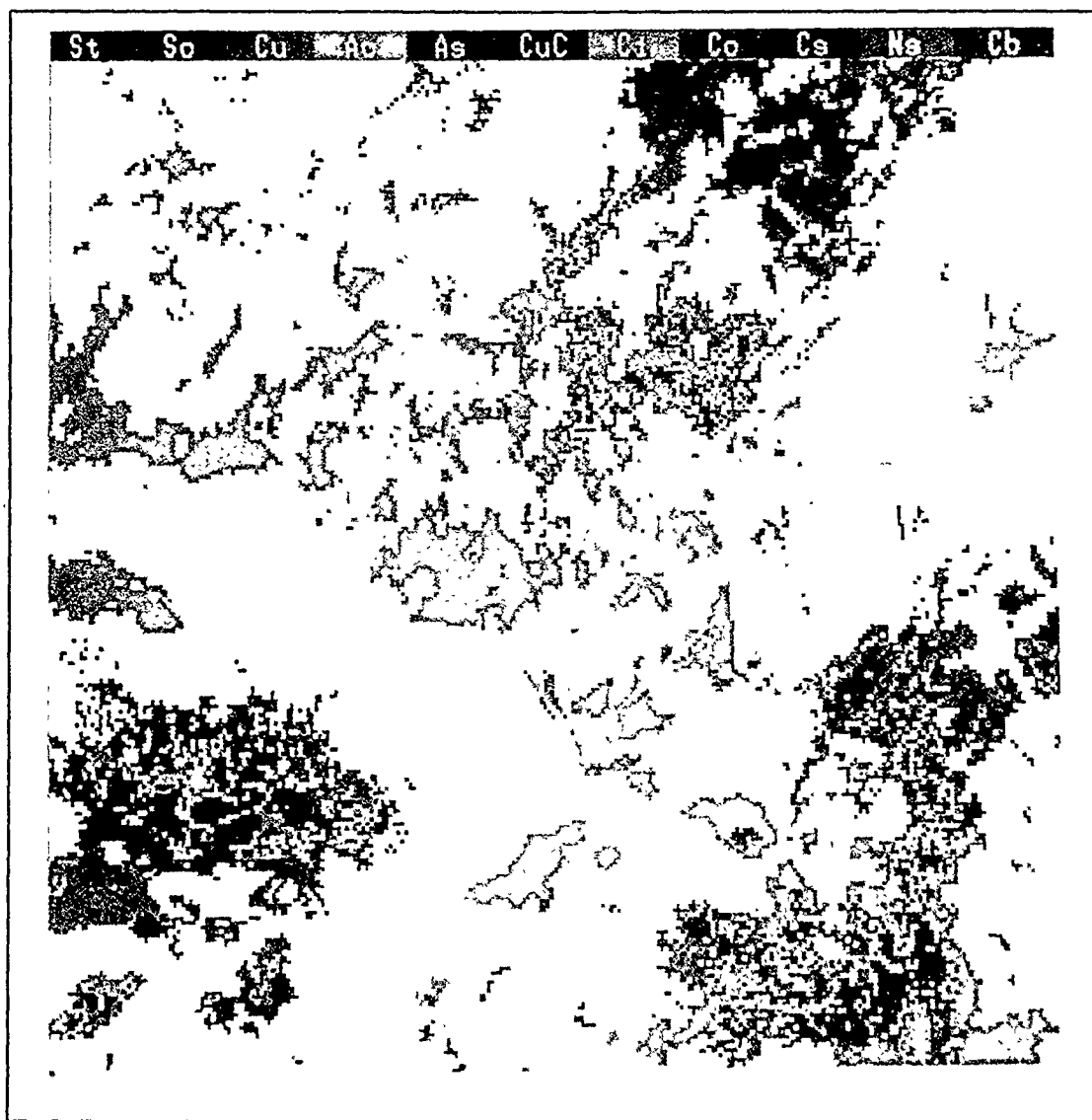
Fig. 14.    Case 1 automated cloud classification results.    Color-coded image for
eleven cloud types analyzed 1809 UTC 13 December 1988.

Results for specific cloud types at each of the verification locations is shown in Table 8. Direct agreement between the automated and manual analysis occurred in 71% of the comparisons. The main discrepancy found is that manually interpreted low clouds are being classified as middle clouds by the model. Manually estimated stratus, stratocumulus and cumulus were respectively analyzed as being altostratus, altocumulus and cumulus congestus by the model. This indicates that the albedo and statistical texture thresholds are correct, but that the temperature threshold separating low from middle clouds is causing the discrepancy. There was little temperature variation from the sounding in this case (Fig. 7), so a certainty in the cloud height estimation is not a problem. Cloud top heights, computed by comparing temperatures obtained from the infrared image with the average vertical temperature profile, range from 3000 to 5000 m for the cloud types in question. Thus, the NPS model classification is consistent with of the conceptual model used in differentiating low from middle clouds. Less significant discrepancies occur with manually analyzed stratus and cirrus being classified by the model as stratocumulus and cirrostratus, respectively. The differentiation between these cloud types based on a textural shift can be subtle to the manual analyst. No one adjustment to the model provides a solution in this instance without causing other, more severe, problems.

Table 8. CASE 1 CLOUD TYPE RESULTS: Automated (column) versus Consensus (row) for each of the eleven cloud types analyzed.

| Type | Clr | St | Sc | Cu | Ac | As | CuC | Ci | Cc | Cs | Ns | Cb |
|------|-----|----|----|----|----|----|-----|----|----|----|----|----|
| Clr  | 8   |    |    |    |    |    |     |    |    |    |    |    |
| St   |     |    | 3  |    |    | 2  |     | 1  |    |    |    |    |
| Sc   |     |    | 2  |    | 1  |    |     |    |    |    |    |    |
| Cu   |     |    |    | 11 |    |    | 2   |    |    |    |    |    |
| Ac   |     |    |    |    |    |    |     |    |    |    |    |    |
| As   |     |    |    |    |    |    |     |    |    |    |    |    |
| CuC  |     |    |    |    |    |    |     |    |    |    |    |    |
| Ci   |     |    |    |    |    |    |     | 14 |    |    |    |    |
| Cc   |     |    |    |    |    |    |     |    |    |    |    |    |
| Cs   | 1   |    |    |    |    |    |     | 4  |    |    |    |    |
| Ns   |     |    |    |    |    |    |     |    |    |    |    |    |
| Cb   |     |    |    |    |    |    |     |    |    |    |    |    |

Table 9 portrays the general results between the manual and model cloud type analysis. Excellent agreement is found between the two classification processes for all cases except middle clouds. Agreement is 89% for clear, 100% for low clouds and 95% for high clouds. Middle clouds show a 0% agreement, as all model analyzed middle cloud was classified as low clouds in the manual analysis. No statistics could be compiled for precipitation cloud types as none were classified by either the manual or model process at the verification points.

Table 9. CASE 1 GENERAL RESULTS: Automated (column) versus Consensus (row) for clear, low (St, Sc, Cu), middle (Ac, As, CuC), high (Ci, Cc, Cs) and precipitation (Ns, Cb) cloud types. Model % agreement is also provided.

| Type | Clear | Low | Middle | High | Precip |
|------|-------|-----|--------|------|--------|
| Clear | 8 | | | | |
| Low | | 16 | 5 | 1 | |
| Middle | | | | | |
| High | 1 | | | 18 | |
| Precip | | | | | |
| *Agree (%)* | *89* | *100* | *0* | *95* | *-* |

## B. CASE 2

The automated NPS cloud analysis image for Case 2 is depicted in Fig. 15. Evaluation is based on manual and model classifications at 33 pixel locations within the subscene. The color enhanced image clearly distinguishes between the wide variety of cloud types present in the subscene. Input AVHRR imagery for the case was presented in Fig. 8. The cyclone's thick cirrus shield with embedded convection and enhanced cumuliform clouds trailing along the frontal boundary is readily identifiable from the color code. Low stratus and stratocumulus are seen to the west of the low pressure center, with layered middle clouds dispersed within the storms frontal band and cloud shield to the south through east of the low.

The specific cloud type results are shown in Table 10, with 76% overall agreement between the automated and manual classifications. The most noticeable discrepancies were between middle, precipitation and high clouds. Manually analyzed altocumulus, altostratus and nimbostratus were classified as cirrostratus by the model. The cause is due to the close proximity of the cloud elements analyzed to the infrared temperature

Fig. 15.  Case 2 automated cloud classification results.  Color coded image for eleven cloud types analyzed 2256 UTC 17 January 1988.

and albedo thresholds forming the boundary between the respective cloud types in the NPS model scheme. Instances of manually analyzed stratocumulus and altostratus being classified as altocumulus and nimbostratus, respectively, is again due to the closeness of the specific cloud top temperatures to the 2500 and 6500 m height temperature thresholds values.

Table 10. CASE 2 CLOUD TYPE RESULTS: Automated (column) versus Consensus (row) for each of the eleven cloud types analyzed.

| Type | Clr | St | Sc | Cu | Ac | As | CuC | Ci | Cc | Cs | Ns | Cb |
|------|-----|----|----|----|----|----|-----|----|----|----|----|----|
| Clr | 5 | | | | | | | | | | | |
| St | | | | | | | | | | | | |
| Sc | | | 2 | | 1 | | | | | | | |
| Cu | | 1 | | 3 | | | | | | | | |
| Ac | | | | | | | | | | 1 | | |
| As | | | | | | 2 | | | | 1 | 1 | |
| CuC | | | | | | | 4 | | | | | |
| Ci | | | | | | | | 2 | | | | |
| Cc | | | | | | | | | | | | |
| Cs | | | | | | | | | | 2 | | |
| Ns | | | | | | | | | | 2 | | 1 |
| Cb | | | | | | | | | | | | 5 |

An interesting finding from this case is the relationship between complex cloud formations and large solar zenith angle. Although the visual imagery is scaled by the solar zenith angle in an attempt to standardize the albedo thresholds, it does not take into account shadowing caused by convective towers when the sun is low on the horizon. Shadowing behind towering convective clouds results in lower albedo values than expected for the shaded portion of the cloud. Cirrostratus or altostratus present in the shadowed region could be classified as cirrus by the model due to the lower albedo value. A related problem arises when the sides of the convective towers appear brighter than the cloud top, due to the angle of solar radiance. This results in misalignment of the brightest portion of the convective cloud and the coldest temperature. Cumulonimbus or cumulus congestus could be classified as cirrocumulus or altocumulus, respectively, because the highest albedo and coldest temperature pixels do not coincide.

35

General results are presented in Table 11, highlighting the models strengths and weaknesses. The overall model performance is very good, with 100% agreement between classifications for clear and low clouds. 86% agreement is found for middle and precipitation cloud types, while 50% match for the high cloud types. No apparent trends in misclassifications can be linked to shadowing near or misalignment of brightest/coldest locations for convective clouds.

Table 11. **CASE 2 GENERAL RESULTS:** Automated (column) versus Consensus (row) for clear, low (St, Sc, Cu), middle (Ac, As, CuC), high (Ci, Cc, Cs) and precipitation (Ns, Cb) cloud types. Model % agreement is also provided.

| Type | Clear | Low | Middle | High | Precip |
|------|-------|-----|--------|------|--------|
| Clear | 5 | | | | |
| Low | | 6 | 1 | | |
| Middle | | | 6 | 2 | 1 |
| High | | | | 4 | |
| Precip | | | | 2 | 6 |
| *Agree (%)* | *100* | *100* | *86* | *50* | *86* |

## C. CASE 3

Case 3 color enhanced cloud types (Fig. 16) provide an easily interpreted image, enabling one to form a conceptual model of the developing shortwave. A total of 57 locations were used in comparing the manual and model classifications. The variety of cloud types present in the subscene provides an excellent data set for the study. The effect that solar zenith angle has on the classification can be obtained through a comparison with Case 2. Both cases are located at approximately the same latitude (34°), but Case 2 has a larger solar zenith angle (55°) than this case study (39°).

Table 12 provides results for the specific cloud types analyzed by the two classification processes. Agreement between the manual and model interpretations is 63%, with the main discrepancies falling into two main categories. The first discrepancy lies in manually classified cumulonimbus being interpreted as nimbostratus by the model, with approximately half of those observed in the verification process matching. Another discrepancy occurs with manually identified low and high clouds being typed as middle clouds by the model. Manually analyzed stratocumulus and cirrocumulus were typed as altocumulus by the model, indicating that the albedo and texture thresholds values
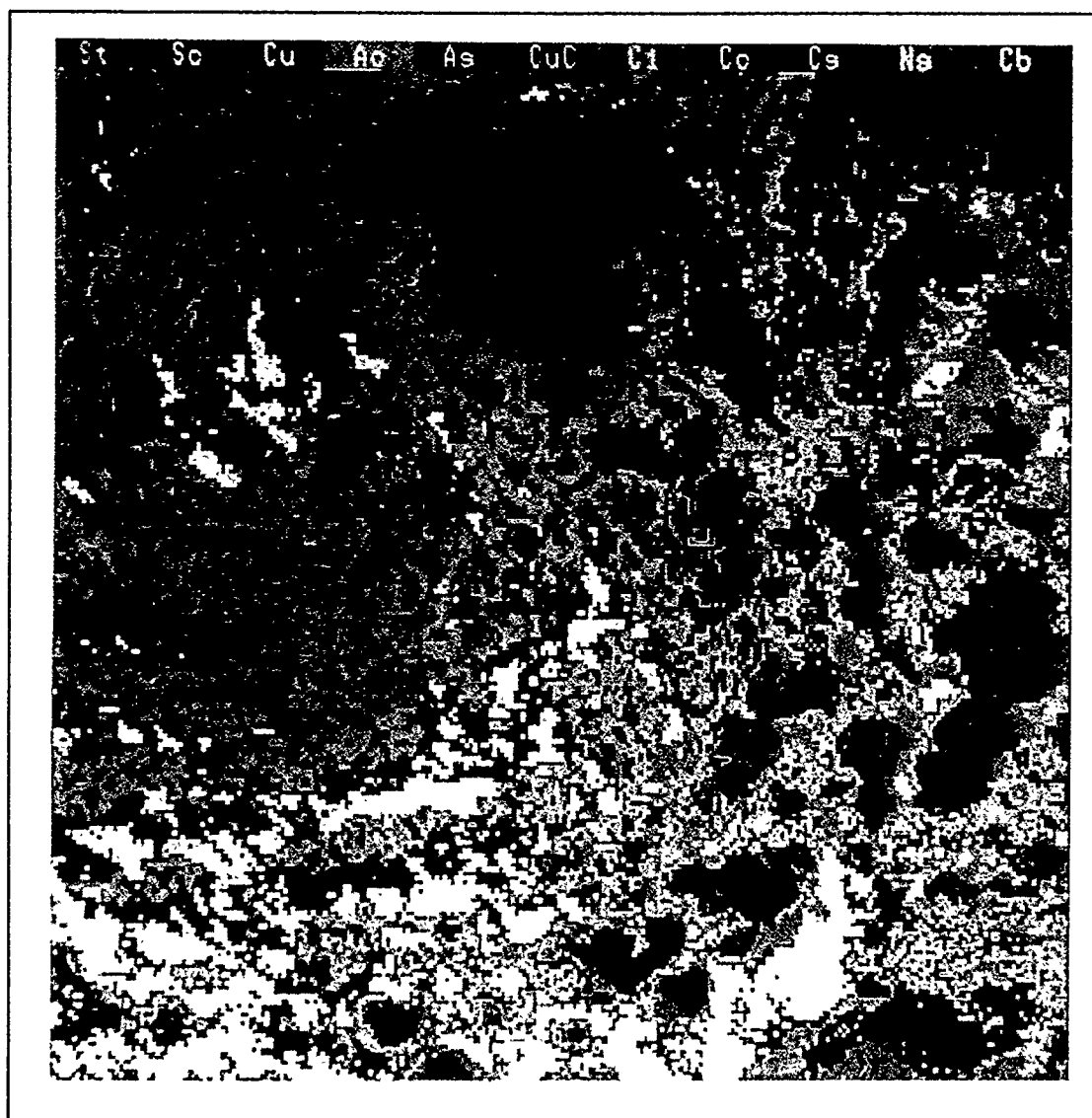
36

Fig. 16.    Case 3 automated cloud classification results.    Color coded image for
eleven cloud types analyzed 1809 UTC 13 December 1988.

37

were reasonable, but that cloud top temperatures used for the classifications were different. The range of heights computed for the cloud tops of model identified altocumulus is 3200 to 5400 m, indicating that the model results are representative of the temperature thresholds set.

Table 12. CASE 3 CLOUD TYPE RESULTS: Automated (column) versus Consensus (row) for each of the eleven cloud types analyzed.

| Type | Clr | St | Sc | Cu | Ac | As | CuC | Ci | Cc | Cs | Ns | Cb |
|------|-----|----|----|----|----|----|----|----|----|----|----|----|
| Clr | 2 | | | | | | | | | | | |
| St | | | 1 | | | 2 | | | | | | |
| Sc | | | 3 | | 2 | | | | | | | |
| Cu | | | 1 | 10 | | | | | | | | |
| Ac | | | | | | | | | | | | |
| As | | | | | | 2 | | 1 | | | | |
| CuC | | | | | | | 5 | | | | | |
| Ci | | | | | 1 | 1 | | 3 | | 1 | | |
| Cc | | | | | 1 | 1 | | | 2 | | | |
| Cs | | | | | | | | | | 1 | | |
| Ns | | | | | | 1 | | | | | 6 | 1 |
| Cb | | | | | | | 2 | | | | 5 | 2 |

Manually analyzed stratus, nimbostratus and cirrus were interpreted as altostratus by the model, with the cloud top height range of the altostratus extending from 3400 to 6400 m. The model results are again more representative of the conceptual model used in separating low, middle and high cloud types. Although change to temperature threshold five will rectify disagreement between nimbostratus and cumulonimbus, changes to the others will only cause larger discrepancies between the two classifications. The 5 K variation between individual rawinsonde and dropwinsondes (Fig. 11) may also cause discrepancies in the model and manual classifications. The average temperature profile used in computing the generalized thresholds may not represent the localized vertical temperature variations present in a baroclinic system. Cloud top temperatures for a particular cloud element may be misclassified between low and middle cloud types, as well as middle and high cloud types, due to deviations present from the average temperature profile.

38

Table 13 presents the general results for the case, providing guidance on the basic performance of the model. Excellent results were obtained for clear, low clouds and precipitating clouds, where 100% agreement between classifications occurred. Manual and model classifications for high clouds agreed 88% of the time, while only 39% of the middle clouds matched. No significant bias can be determined between the results from this case and those in Case 2. This suggests that the standardizing process used on the albedos is successful.

Table 13. CASE 3 GENERAL RESULTS: Automated (column) versus Consensus (row) for clear, low (St, Sc, Cu), middle (Ac, As, CuC), high (Ci, Cc, Cs) and precipitation (Ns, Cb) cloud types. Model % agreement is also provided.

| Type | Clear | Low | Middle | High | Precip |
|------|-------|-----|--------|------|--------|
| Clear | 2 | | | | |
| Low | | 15 | 4 | | |
| Middle | | | 7 | 1 | |
| High | | | 4 | 7 | |
| Precip | | | 3 | | 14 |
| Agree (%) | 100 | 100 | 39 | 88 | 100 |

## D. CASE 4

Fig. 17 shows the automated model image for Case 4, with the color enhancement clearly differentiating between the layered low, middle and high cloud decks present in the mid-latitude subscene. Comparison of the manual and model classification is based on 48 verification locations. The dominant cloud types are low and high cloud types, with some middle clouds present. The fine distinction between the extensive low cloud deck and interdispersed middle clouds seems to be handled adequately by the model. Precipitation clouds are not well represented in the subscene.

Specific results for the verification locations are presented in Table 14. The overall agreement is fair, with 54% of the classifications matching. Direct agreement statistics suffer in this case primarily because of discrepancies in low cloud analysis. A majority of manually classified cumulus were analyzed as stratus by the model. Model results would conform more with the manual interpretation in this instance by lowering the statistical texture threshold value for stratus, cumulus differentiation to 0.03. Manually classified stratus were often analyzed as stratocumulus by the model. Although the
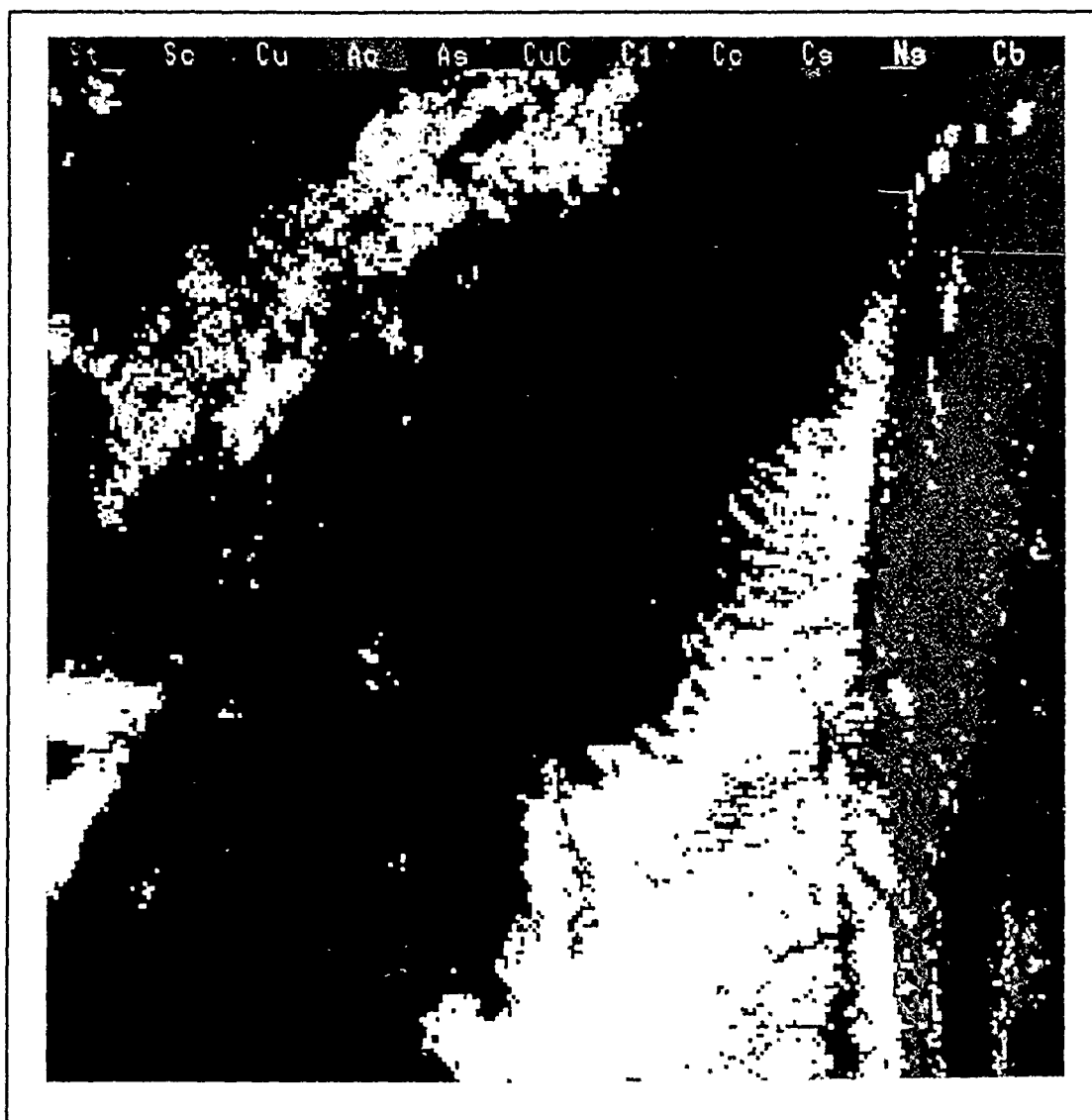
Fig. 17. Case 4 automated cloud classification results. Color coded image for eleven cloud types analyzed 1758 UTC 14 December 1988.

distinction between these cloud types can be subtle, better agreement can be obtained by raising the second temperature threshold to 1800 m. Model classified stratocumulus were also identified as both middle clouds (left sector of image) and cirrus (right sector of image) by the manual analysts. The cloud top heights were calculated to be less than 2500 m in these instances, indicating that the model conforms with the set temperature threshold. Slightly better agreement can be obtained by lowering the height at which the third temperature threshold value is obtained to 2000 m. Additional discussion on shifting threshold values is summarized below.

Table 14. CASE 4 CLOUD TYPE RESULTS: Automated (column) versus Consensus (row) for each of the eleven cloud types analyzed.

| Type | Clr | St | Sc | Cu | Ac | As | CuC | Ci | Cc | Cs | Ns | Cb |
|------|-----|----|----|----|----|----|-----|----|----|----|----|----|
| Clr | 2 | 1 | | | | | | | | | | |
| St | | 9 | 5 | | | | | | | | | |
| Sc | | 1 | 1 | 1 | | | | | | | | |
| Cu | | 5 | | 1 | | | | | | | | |
| Ac | | | 1 | | 1 | | | | | | | |
| As | | | 2 | | | 3 | | | | | | |
| CuC | | | 1 | | | | | | | | | |
| Ci | | | 2 | | | | | 3 | | | | |
| Cc | | | | | | | | | 4 | 1 | | |
| Cs | | | | | | | | 2 | | 2 | | |
| Ns | | | | | | | | | | | | |
| Cb | | | | | | | | | | | | |

Another possible cause for the discrepancies between model and manually identified low and middle clouds is the 7 K temperature variation at low levels between individual rawinsondes (Fig. 13). The average vertical temperature profile used by the model may not be representative of each sector within the total subscene. Temperature deviations on the order of magnitude noted could cause misclassifications by the model. However, it should be noted that the three rawinsondes and gridded profile are located within the central portion of the image, where the majority of low and middle discrepancies occurred. The average temperature profile provides an acceptable representation of the mesoscale temperature variations present.

Much better agreement is found for the general results presented in Table 15. The NPS model agrees with the manual classification 100% for clear conditions, middle and high clouds. 77% agreement is found between low clouds, while no statistics were compiled for precipitation clouds, as none were verified by either classification scheme. These results indicate that although the model suffered in direct comparison between specific cloud types, it did an excellent job in portraying the general cloud characteristics within the subscene.

Table 15. CASE 4 GENERAL RESULTS: Automated (column) versus Consensus (row) for clear, low (St, Sc, Cu), middle (Ac, As, CuC), high (Ci, Cc, Cs) and precipitation (Ns, Cb) cloud types. Model % agreement also provided.

| Type | Clear | Low | Middle | High | Precip |
|------|-------|-----|--------|------|--------|
| Clear | 2 | 1 | | | |
| Low | | 23 | | | |
| Middle | | 4 | 4 | | |
| High | | 2 | | 12 | |
| Precip | | | | | |
| *Agree (%)* | *100* | *77* | *100* | *100* | *-* |

## E. COMPOSITE RESULTS

A composite representation of the classifications obtained in the four detailed studies is presented. This is accomplished by adding the number of each particular manual and model classification from each of the four case studies into a single matrix. The results portray the overall NPS model performance for different latitudes and solar zenith angles using the generalized threshold scheme developed. Table 16 shows the specific results for the 11 cloud types analyzed, based on the total of 187 pixel locations within the four case studies. Overall agreement between the expert manual cloud analysis and automated model analysis is 67%.

The following findings represent the main discrepancies between the manual and model interpretation of specific cloud types. Manually interpreted cumulus were classified as stratus by the model, indicating that the statistical textural standard deviation value separating these two cloud types is too small. A value of 0.03 for this threshold, instead of 0.05, will bring the two classifications toward a higher percentage of agreement.

42

Table 16. COMPOSITE OF CLOUD TYPE RESULTS: Automated (column) versus Consensus (row) for each of the eleven cloud types analyzed.

| Type | Clr | St | Sc | Cu | Ac | As | CuC | Ci | Cc | Cs | Ns | Cb |
|------|-----|----|----|----|----|----|-----|----|----|----|----|----|
| Clr | 17 | 1 | | | | | | | | | | |
| St | | 9 | 9 | | | 4 | | 1 | | | | |
| Sc | | 1 | 8 | 1 | 4 | | | | | | | |
| Cu | | 6 | 1 | 25 | | | 2 | | | | | |
| Ac | | | 1 | | 1 | | | | | 1 | | |
| As | | | 2 | | | 7 | | 1 | | 1 | 1 | |
| CuC | | | 1 | | | | 9 | | | | | |
| Ci | | | 2 | | 1 | 1 | | 22 | | 1 | | |
| Cc | | | | | 1 | 1 | | | 6 | 1 | | |
| Cs | 1 | | | | | | | 2 | | 9 | | |
| Ns | | | | | | 1 | | | | 2 | 6 | 2 |
| Cb | | | | | | | 2 | | | | 5 | 7 |

Manually classified stratus and middle clouds were analyzed as stratocumulus by the NPS model, indicating that the height of the second infrared temperature threshold is set slightly too low, while the third infrared temperature threshold is set too high. However, this is contradicted by the fact that manually identified stratocumulus are often classified as altocumulus by the by the NPS model, suggesting that the third infrared temperature threshold should be obtained from a higher height, not lower. These two discrepancies tend to negate each other, and thus the third temperature threshold should be left at 2500 m for optimum agreement between the manual and model classification. The second temperature threshold can be raised to 1800 m in order to obtain better agreement between manually analyzed stratus and model analyzed stratocumulus. The new threshold height still conforms to the conceptual model used in distinguishing stratus from stratocumulus clouds. It should also be noted that a majority of the discrepancies between low and middle cloud types occurred due to manually classified low clouds with tops above 2500 m and middle clouds with tops below 2500 m.

The final significant discrepancy is that model classified nimbostratus was identified as cumulonimbus by the manual analysts. This indicates that either the fifth infrared temperature threshold is obtained at too great a height, or that another discriminant test

43

is required for differentiation of these cloud types. Lowering the height at which the temperature threshold is obtained to 7000 m results in better agreement between the manual and model analysis, and still fits conceptually.

It should be stressed that by changing the threshold values used in the model to increase agreement between one set of cloud types for a particular subscene can cause greater disagreement between other interrelated cloud type classifications. Optimum classification agreement between manual and model results can only be realized by treating each case as a localized variation to the generalized threshold scheme. Only by employing localized deviations, within the range of threshold values stated previously, can maximum correlation between manual and NPS model be obtained for each case. The use of a single average temperature profile as being representative of each subscene may also be misleading, especially in baroclinic systems. Incorporating separate temperature profiles for individual sectors within the subscene may provide more accurate classifications by the NPS model.

General results for the composite study are presented in Table 17. The NPS model agreement with the expert manual classification is 94% for clear conditions, 90% for low clouds, 50% for middle clouds, 87% for high clouds and 95% for precipitation cloud types. These results indicate that the model does a very good job in classifying the basic cloud types when using the set of generalized thresholds. The main discrepancy lies in the accurate NPS model classification of middle clouds. Since an approximate equal number of manually classified low and high cloud types were analyzed by the model as being middle clouds, no simple solution is available to rectify the problem. Any variation to the third and fourth infrared temperature threshold would only cause greater problems for the other cloud types analyzed.

Table 17. **COMPOSITE OF GENERAL RESULTS:** Automated (column) versus Consensus (row) for clear, low (St, Sc, Cu), middle (Ac, As, CuC), high (Ci, Cc, Cs) and precipitation (Ns, Cb) cloud types. Model % agreement is also provided.

| Type | Clear | Low | Middle | High | Precip |
|---|---|---|---|---|---|
| Clear | 17 | 1 | | | |
| Low | | 60 | 10 | 1 | |
| Middle | | 4 | 17 | 3 | 1 |
| High | 1 | 2 | 4 | 41 | |
| Precip | | | 3 | 2 | 20 |
| *Agree (%)* | *94* | *90* | *50* | *87* | *95* |

45

# VI. CONCLUSIONS AND RECOMMENDATIONS

Advances in both computer technology and satellite remote sensing systems over the past decade have provided today's meteorologists with the tools necessary for producing an accurate objective cloud analysis. The need for comprehensive cloud type information is found in a wide variety of disciplines, including military applications. A quick objective technique, such as the NPS model, is desirable as it runs efficiently on a minicomputer, provides global coverage through its use of polar orbiting satellites, and exploits the multispectral characteristics of the NOAA AVHRR sensor. The model can be run on a near real time basis, enabling operational decision making to be based on its output. Implementation of the NPS model into both the Navy's Tactical Environmental Support System (TESS 3) and Air Force's Mark-IVB Tactical Terminal (TACTERM) systems can be easily accomplished.

The NPS model is based on a multispectral scheme, incorporating visual, infrared and infrared temperature difference imagery. The 11 cloud types are distinguished by analyses based on thresholding techniques using albedos, temperature, temperature difference and standard deviation values. A statistical textural analysis is used to differentiate between stratiform and cumuliform cloud types. The model is verified using four indepth case studies obtained during the winters of 1987 and 1988 over the west and east coastal regions of the United States. Subscenes were chosen based on variation of geographic location, large range of solar zenith angle and presence of a wide variety of cloud types. This enables the verification to focus on model performance at different latitudinal locations experiencing a variety of solar zenith angles. A set of generalized threshold values are tested for each case to determine how the model performs in an operational global setting.

Verification is based on direct comparison between the automated NPS model and an expert consensus manual analysis produced by two experienced meteorologists. Locations within each subscene were chosen by the manual analysts in an attempt to portray the characteristic cloud types and patterns within the total image. A variety of cloud types, including those that have posed problems in other automated classifications schemes, were picked to see how the NPS model performs under the most challenging conditions. Both manual and model identified cloud types at these pixel locations are

46

compared and tabulated in a matrix form that allows easy interpretation of the classification's strengths and weaknesses.

A composite description of the NPS model's performance is obtained through a compilation of results obtained in the four independent case studies. Overall agreement between specific cloud types is 67%, with some cloud types matching better between the manual and model analysis than others. Manually analyzed cumulus are often classified as stratus by the model, indicating that the textural threshold value needs slight adjustment for this case. The model tends to classify manually interpreted stratus and stratocumulus as, respectively, stratocumulus and middle clouds. This indicates that some adjustment to the second and third temperature thresholds is needed for the generalized heights at which the temperatures are obtained. Most of the discrepancies between low and middle clouds is due to different heights used by the model and manual analysts in distinguishing between them. The NPS model also tends to classify manually identified cumulonimbus as nimbostratus. Adjustments to the fifth temperature threshold values will bring the manual and model classifications toward better agreement for these cases.

Excellent results are obtained for more general analysis criteria. Clear, low clouds, middle clouds, high clouds and precipitation clouds agree between the manual and model classification 94%, 90%, 50%, 87% and 95% of the time, respectively. Although the generalized threshold values produce very good results for the different latitudinal and solar zenith angle case studies presented, one can obtain even better results by fine tuning the thresholds for localized conditions. A range of threshold values exists which the trained meteorologist can use in order to optimize the objective cloud type analysis for the area of interest. By making the threshold changes suggested in each particular case study, other misclassifications can be manifested between the other cloud types analyzed.

Recommendations for further research in this area include case studies from the spring, summer and fall to evaluate the effect of seasonal variations on the generalized threshold values and increase the statistical data base. Exploitation of the additional spectral channels present on the AVHRR sensor could prove useful in constructing other cloud identification schemes. These may prove helpful in rectifying some of the problem areas identified in this study. Studies involving further investigation of the split window technique for identifying cirrus clouds and differentiating between dense cirrostratus and thick convective cloud types is needed. The use of infrared channel 3 (3.74 $\mu$m) for identifying low clouds at night and separating clouds from snow surfaces (Allen 1987; Barron 1988) could be incorporated easily into the NPS model.

# LIST OF REFERENCES

Allen Jr., A.C., 1987: Automated satellite cloud analysis: A multispectral approach to the problem of snow, cloud discrimination. M.S. Thesis, Naval Postgraduate School, Monterey, CA, 113pp.

Barron, J.P., 1988: An objective technique for arctic cloud analysis using multispectral AVHRR satellite imagery. M.S. Thesis, Naval Postgraduate School, Monterey, CA, 80 pp.

Harris, R., and E.C. Barrett, 1978: Toward an objective nephanalysis. *J. Appl. Meteorol.*, 17, 1258-1266.

Inoue, T., 1987: A cloud type classification with NOAA-7 split-window measurements. *J. Geophys. Res.*, 92, 3991-3999.

Kiess, R.B. and W.M. Cox, 1988: The AFGWC automated real-time cloud analysis model. AFGWC Tech Memo 88/001, AFGWC, Air Weather Service (MAC), Offutt AFB. NE, 82 pp.

Liljas, E., 1982: Automated techniques for the analysis of satellite cloud imagery. *Nowcasting*, ed. K. Browning, Academic Press, London, 177-190.

------, 1984: Processed satellite images for operational forecasting. Swedish Meteorological and Hydrological Institute, 43 pp.

Maurer, H., 1974: Quantification of textures - textural parameters and their significance for classifying crop types from color aerial photographs. *Photogrammmetria*, 30, 21-40.

Moren, C., 1984: Evaluation of the SPADS automated cloud analysis model. M.S. Thesis, Naval Postgraduate School, Monterey, CA, 139 pp.

Nelson, C.A., 1982: Estimation and mapping of cloud and rainfall areas with an interactive computer. M.S. Thesis, Naval Postgraduate School, Monterey, CA, 134 pp.

Reynolds, D.W. and T.H. Vonder Haar, 1976: A bispectral method for cloud parameter determination. *Mon. Wea. Rev.*, 105, 446-457.

Spray, L.A., 1985: Geostationary satellite analyses of precipitation and cloud parameters. M.S. Thesis, Naval Postgraduate School, Monterey, CA, 100 pp.

Wash, C.H., L.A. Spray and L.C. Chou, 1985: Satellite cloud and precipitation analysis using a minicomputer. Tech Report NPS-63-85-003, Naval Postgraduate School, Monterey, CA, 91 pp.

Weszka, J.S., C.R. Dyer and A. Rosenfeld, 1976: A comparative study of texture measures for terrain classification. *IEEE Trans. Syst. Man. Cybern.*, SMC-6, 269-285.

Wyse, N.R., 1984: The inclusion of surface data into the SPADS cloud analysis model. M.S. Thesis, Naval Postgraduate School, Monterey, CA, 145 pp.

# INITIAL DISTRIBUTION LIST

No. Copies

1. Defense Technical Information Center      2
   Cameron Station
   Alexandria, VA  22304-6145

2. Library, Code 0142      2
   Naval Postgraduate School
   Monterey, CA  93943-5002

3. Commander      1
   Air Weather Service
   Scott Air Force Base, IL 62225

4. Commander      1
   Naval Oceanography Command
   Stennis Space Center, MS 39529-5000

5. Commanding Officer      1
   Air Force Global Weather Center
   Offutt Air Force Base, NE 68113-5000

6. Commanding Officer      1
   Fleet Numerical Oceanography Center
   Monterey, CA 93943-5005

7. USAF ETAC LD      1
   Air Weather Service Technical Library
   Scott Air Force Base, IL 62225

8. Commanding Officer      1
   AFIT CIR
   Wright-Patterson Air Force Base, OH 45433-6583

9. Chairman (Code MR)      1
   Department of Meteorology
   Naval Postgraduate School
   Monterey, CA 93943-5000

10. Professor Carlyle H. Wash (Code MR/WX)      8
    Department of Meteorology
    Naval Postgraduate School
    Monterey, CA 93943-5000

11. Professor Forrest R. Williams (Code MR/WF)      1
    Department of Meteorology
    Naval Postgraduate School
    Monterey, CA 93943-5000

12. Professor Philip A. Durkee (Code MR/DE)        1
    Department of Meteorology
    Naval Postgraduate School
    Monterey, CA 93943-5000

13. Commanding Officer        1
    AFGWC/SD
    Offutt Air Force Base, NE 68113

14. Captain Thomas J. Neu        2
    AFGWC/SDDP
    Offutt Air Force Base, NE 68113

15. Commanding Officer        1
    Naval Oceanographic and Atmospheric Research Laboratory
    Monterey, CA 93943-5006